Title

A review on the stability and surface modification of layered transition-metal oxide cathodes

Authors

Kim, Ju-Myung
Zhang, Xianhui
Zhang, Ji-Guang
et al.

Publication Date

2021-06-01

DOI

10.1016/j.mattod.2020.12.017

Peer reviewed

A review on the stability and surface modification of layered transition-metal oxide cathodes

Ju-Myung Kim [1,†], Xianhui Zhang [1,†], Ji-Guang Zhang [1], Arumugam Manthiram [2], Ying Shirley Meng [3], Wu Xu [1,*]

[1] Energy and Environment Directorate, Pacific Northwest National Laboratory, Richland, WA 99354, United States
[2] Department of Mechanical Engineering and Texas Materials Institute, The University of Texas at Austin, Austin, TX 78712, United States
[3] Department of NanoEngineering, Materials Science and Engineering, University of California San Diego, La Jolla, CA 92093, United States

An ever-increasing market for electric vehicles (EVs), electronic devices and others has brought tremendous attention on the need for high energy density batteries with reliable electrochemical performances. However, even the successfully commercialized lithium (Li)-ion batteries still face significant challenges with respect to cost and safety issues when they are used in EVs. From a cathode material point of view, layered transition-metal (TM) oxides, represented by $LiMO_2$ (M = Ni, Mn, Co, Al, *etc.*) and Li-/Mn-rich $xLi_2MnO_3{\cdot}(1–x)LiMO_2$, have been considered as promising candidates because of their high theoretical capacity, high operating voltage, and low manufacturing cost. However, layered TM oxides still have not reached their full potential for EV applications due to their intrinsic stability issues during electrochemical processes. To address these problems, a variety of surface modification strategies have been pursued in the literature. Herein, we summarize the recent progresses on the enhanced stability of layered TM oxides cathode materials by different surface modification techniques, analyze the manufacturing process and cost of the surface modification methods, and finally propose future research directions in this area.

Keywords: Lithium-ion batteries; Cathodes; Layered transition-metal oxides; Stability; Surface modification

Introduction

An ever-increasing market for electric vehicles (EVs), portable electronic devices, drones, internet of things, etc. has brought tremendous attention to the need for high energy density batteries with reliable electrochemical performances. EVs, especially, are penetrating transportation worldwide market in an increased rate due to their high energy efficiency and environmental benefits. The total number of global electric cars exceeded 5.1 million in 2018, an increase of 62% from 2017, and is expected to reach 23 million in the New Policies Scenario in 2030 [1]. Driving range, price, and safety are always the primary concerns for EV markets. Therefore, improving specific energy, power density, cycling stability, calendar life, and safety, while reducing the cost of lithium (Li)-ion batteries (LIBs) (which are the dominant power source for EV propulsion) become increasingly imperious. However, cathode materials, the largest component by both weight and cost in state-of-the-art LIBs, are still the main bottleneck to reach these goals [2].

An ideal cathode for EV LIBs should exhibit the following features: (1) high operating voltage; (2) high reversible capacity; (3) high electronic/ionic conductivities to ensure high power density; (4) suitable structural stability for continuous Li^+ de-intercalation and intercalation; (5) good compatibility with electrolyte to ensure cycling stability, calendar life, and safety; and (6) affordable price of raw materials and facile synthesis [3–6]. Generally, cathode materials can be structurally categorized as layered, spinel, and olivine types, among which, layered

* Corresponding author.
E-mail address: Xu, W. (wu.xu@pnnl.gov)
† These authors contributed equally to this work.

transition-metal (TM) oxides have solidified their status as the major choice of cathode materials in LIBs for EVs today [7,8]. Here, layered TM oxides refer to $LiMO_2$ (M = Ni, Mn, Co, Al, etc., LMO) and Li-/Mn-rich xLi_2MnO_3-(1–x)$LiMO_2$ (LMR). LMO cathodes have been widely developed for commercial LIBs due to their comprehensive advantages regarding theoretical capacity, operating voltage, and manufacturing cost [9,10]. LMR layered oxides are regarded as one of the most promising cathodes and have attracted increasing attention in recent years due to the high theoretical capacity of $\geq$280 mAh g^{-1} and a high working potential of ~3.7 V, thus a high gravimetric energy density of ~900 Wh kg^{-1} [11–13].

Despite the promising progress over the past years, these technologically important cathode materials have not yet fully met the expectation for EV applications due to their intrinsically physical and chemical drawbacks, as well as the dynamic structural transition during the electrochemical processes. First, the intrinsic instabilities in the delithiated state of the layered TM oxides, including side reactions with electrolytes, phase transition, structural degradation, TM cation dissolution, oxygen (O) evolution, and cracking, considerably contribute to the voltage and capacity decay and limited cycle life, which greatly hinder their full success [14–18]. Especially, the side reaction on the surface of the layered TM oxides with the electrolyte triggers others. Residual moisture existing in the electrolyte hydrolyzes $LiPF_6$ to generate hydrofluoric acid (HF), which can attack the surface of the layered TM oxides, leading to TM cation dissolution. In addition, the electrolyte penetration from the surface to the inside of cathode particles severely damages the structure and causes cracking. Second, gas generation, mainly originating from the decomposition of residual Li species, such as Li_2CO_3 and LiOH on the cathode particle surface [19–21], and oxygen release from the cathode material, leads to performance deterioration and safety issues [22–24]. With the emergence of anionic redox reaction ($O^{2-} \rightarrow O^{2n-}$) in LMR as a new paradigm to increase the energy density, oxygen redox is always accompanied by irreversible oxygen release mainly at the surface, leading to inferior rate capability and serious voltage and capacity fade, and even triggering a thermal runaway event [25–27]. Third, the sensitivity to air and moisture exposure makes the storage of LMO a hassle practically [28,29]. Besides, the residual Li species generated by exposure to air and moisture could act as conductive barriers on the surface. Last but not least, kinetic processes including Li^+ and electron transport and interfacial ion transfer are also key factors in controlling the rate capability, polarization, and usable capacity of the layered TM cathodes [30–32].

Global efforts have been devoted to addressing the above mentioned issues, and surface modification has been proven to be one of the most promising approaches. Scheme 1 summarizes the issues deriving from the surface instabilities of LMO and LMR cathode materials and the corresponding remedying approaches reported in the literature. The cathode surface is chemically/electrochemically active, which makes it severely prone to various stability problems when in direct contact with the electrolyte. As summarized in Tables 1–4, which are categorized by the types of materials, surface control can be multi-functional and act as inhibitors of phase transition, oxygen release and gas generation, protective barriers for electrolyte decomposition and TM dissolution, mechanical buffers, moisture and air shields, HF scavengers, and electronic/ionic conductivity facilitator, greatly enhancing the energy density, rate capability, cycle life, and safety [33]. Defining the chemical/physical/structural changes of the outer and inner surfaces as surface modification, three types can be categorized: (1) surface coating, the dominant strategies, including electrochemically inactive compounds coating (*e.g.*, metal oxides, fluorides, and phosphates) [34–38], Li impurities-reactive coating (Co_3O_4) [39] and Li-reactive coating (MoO_3) [40], Li ion conductive coating ($LiTi_2O_4$, Li_2ZrO_3 and $Li_4Mn_5O_{12}$) [41–43], conducting polymer coating (*e.g.*, polypyrrole (PPy), polyaniline (PANI) and poly(3,4-ethylenedioxythiophene) (PEDOT)) [44–46], and other materials coatings, such as MXene (e.g. $Ti_3C_2T_x$) [47] and conductive graphene matrix [48]; (2) gradient structure design, including core–shell structures [49–52], hierarchical architectures (*i.e.,* multi-shell) [53–55], and concentration gradient (CG) structures [56–58]; and (3) other surface treatments, such as rinsing with water to form an oxygen-depleted surface layer [59,60], utilizing atomic surface reduction to alter the electronic structure of the surface [61], and surface doping to form an enriched extrinsic ions surface [62].

There are a few review papers summarizing the issues and mitigation approaches for Ni-rich layered TM oxides or Li-/Mn-rich layered TM oxides in the past years [14,17,18,63–67]. We provide in this review a more comprehensive account of the strategies employed in a unified manner for both Ni-rich and Li-/Mn-rich layered TM oxides, which are promising cathode candidates for LIBs and Li metal batteries, considering the work during the past decade. With the understanding of the roles of surface control in improving the electrochemical performances, we discuss the criteria for proper designs of surface modifications regarding every intrinsic interfacial issue. Finally, we present our perspective on the future strategies being suitable for realizing a maximized surface protection of layered TM oxide cathode materials to meet the requirements for EV power sources in view of process and cost.

Surface modification strategies to mitigate the stability issues

Coating the surface of cathode particles with certain materials is considered to be an easy and effective way to prevent side reactions. Most of the coating materials basically have a physical protection effect that reduces the direct contact of cathode particle surface with the electrolyte. Further, to avoid the limitation of inhibiting charge transfer on the cathode surface by the coating layer, an optimized content of the coating material and a homogeneous coating morphology are required. Based on the coating materials applied for surface modification of the cathode materials, shown in Tables 1–4, their functions are discussed in the following sections.

Strategies for reducing side reactions with electrolyte

HF scavenging

Trace amount of HF is always present in conventional $LiPF_6$-based liquid electrolytes because residual moisture is inevitable in liquid electrolytes and the $LiPF_6$ salt is easily hydrolyzed through reaction (1):

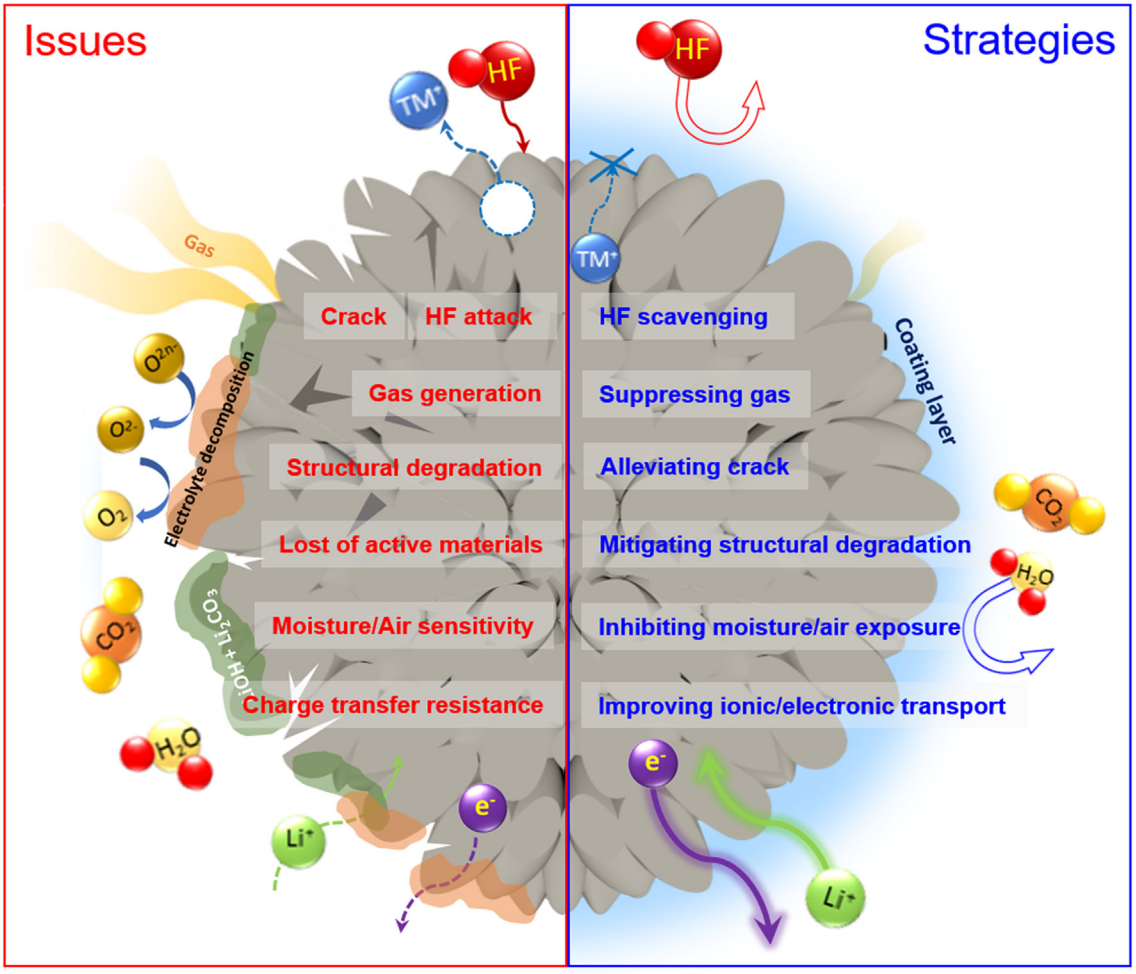

SCHEME 1

Schematic illustration of the stability issues and the surface modification strategies.

$$LiPF_6 + H_2O \rightarrow LiF\downarrow + POF_3 + 2HF \quad (1)$$

In addition, the high surface area electrodes also adsorb some moisture during electrode and cell fabrication processes, which is hard to be removed. Therefore, when the $LiPF_6$-based electrolyte contacts moisture on electrode surfaces, more HF may be formed. On the other hand, HF can also be generated through reactions (2) and (3) at elevated temperatures:

$$LiPF_6 \rightarrow LiF\downarrow + PF_5 \quad (2)$$

$$PF_5 + H_2O \rightarrow POF_3 + 2HF \quad (3)$$

It is well known that acidic species like HF in electrolytes can attack the surface of TM oxide cathode materials, triggering the dissolution of TM ions and capacity decay by the generation of more soluble byproducts on the surface of the cathode as shown in reactions (4), (5) and (6). Additionally, the TM ions dissolved in electrolytes will move to and deposit on the surface of anode, leading to increased cell resistance [15,68–70].

$$MnO + 2HF \rightarrow MnF_2 + H_2O \quad (4)$$

$$CoO + 2HF \rightarrow CoF_2 + H_2O \quad (5)$$

$$NiO + 2HF \rightarrow NiF_2 + H_2O \quad (6)$$

To solve this issue, HF scavenging materials, which are mainly based on the reaction with HF, have been widely employed to form a coating layer on the surface of TM layered cathodes. TiO_2 and SiO_2 are considered as good HF scavengers through the following reactions accompanying with the formation of Ti/Si–O–F and/or Ti/Si–F layers:

$$TiO_2 + 4HF \rightarrow TiF_4 + 2H_2O \quad (7)$$

$$SiO_2 + 4HF \rightarrow SiF_4 + 2H_2O \quad (8)$$

$$SiO_2 + 6HF \rightarrow H_2SiF_6 + 2H_2O \quad (9)$$

TiO_2 coated $LiNi_{0.6}Co_{0.2}Mn_{0.2}O_2$ (NCM622) [71] and $LiNi_{0.8}Co_{0.15}Al_{0.05}O_2$ (NCA) [72] exhibit improved cycling performance even at high temperature (55 °C) after coating (Table 1), benefiting from the HF scavenging ability of TiO_2. Cho et al. [73] indicated that the SiO_2 coating layer on the surface of NCM622 shows a superior absorption of HF, being effective in improving cycle life even though with an electrolyte containing 1000 ppm of water. SiO_2 coated $Li_{1.2}Ni_{0.2}Mn_{0.6}O_2$ cathode showed remarkably improved cycling stability compared to the bare one in electrolytes with 1000 and 2000 ppm water separately due to the HF scavenging capability of SiO_2 [74]. However, the abovementioned oxide-type HF scavengers are based on their sacrificial

TABLE 1

Summary of the surface modification using metal oxides.

Coating material	Function	Cathode active material	Mass loading [mg cm^{-2}]	Voltage range [V vs. Li/Li$^+$]	Electrolytes	Capacity retention after × cycles at charging/discharging C-rate	Capacity [mAh g^{-1}] at discharging C-rate	Ref.
Al_2O_3	Thermal stability, Mitigating structural degradation	$LiNi_{0.8}Co_{0.15}Al_{0.05}O_2$		2.8–4.4	1 M $LiPF_6$ EC/EMC/DMC (1:1:1 v/v/v)	90.0%,100th at 1C/1C		[112]
	Mitigating structural degradation	$LiNi_{0.5}Mn_{0.3}Co_{0.2}O_2$		3.0–4.5	1 M $LiPF_6$ EC/DEC/EMC (1:1:1 v/v/v)	85.0%, 100th at 0.5C/0.5C		[113]
	Mitigating structural degradation, Alleviating crack generation	$LiNi_{1/3}Co_{1/3}Mn_{1/3}O_2$			1 M $LiPF_6$ EC/EMC/DMC (1:1:1 v/v/v)	96.0%,100th at 1C/1C		[114]
	Alleviating crack generation			3.0–4.3	1 M $LiPF_6$ EC/DEC (1:1 v/v)	92.0%, 70th at 1C/1C (55 °C)		[148]
Co_3O_4	Suppressing gas generation	$LiNi_{0.8}Co_{0.15}Al_{0.05}O_2$		2.8–4.3		91.6%, 100th at 1C/1C		[39]
TiO_2	HF scavenging	$LiNi_{0.6}Co_{0.2}Mn_{0.2}O_2$		2.5–4.3		85.9%, 100th at 1C/1C; 80.8%, 100th at 1C/1C (55 °C)		[71]
		$LiNi_{0.80}Co_{0.15}Al_{0.05}O_2$		2.8–4.5	1 M $LiPF_6$ EC/DMC (1:1 w/w)	90.2%, 100th at 1C/1C; 73.2%, 100th at 1C/1C (55 °C)		[72]
	Mitigating structural degradation	$LiCoO_2$		3.0–4.4		98.4%, 50th at 1C/1C		[121]
				3.0–4.5	1 M $LiPF_6$ EC/DMC (1:1 v/v)	86.5%, 100th at 1C/1C		[122]
	Improving ion transport	$Li_{1.2}Mn_{0.54}Co_{0.13}Ni_{0.13}O_2$		2.0–4.8		82.1%, 200th at 0.5C/0.5C	200.1 at 5C	[47]
SiO_2	HF scavenging	$LiNi_{0.6}Co_{0.2}Mn_{0.2}O_2$		3.0–4.3	1 M $LiPF_6$ EC/DMC (1:2 v/v)	97.0%, 50th at 0.5C/0.5C		[73]
SiO_2	HF scavenging, Thermal stability	$Li_{1.2}Ni_{0.2}Mn_{0.6}O_2$		2.0–4.8	1 M $LiPF_6$ EC/DMC (1:1 v/v)			[74]
SnO_2	Thermal stability	$LiNi_{0.5}Co_{0.2}Mn_{0.3}O_2$	4.0	2.8–4.5	1 M $LiPF_6$ EC/DEC (3:7 v/v) +5wt.% LiDFOB	93.4%, 100th at 1C/1C		[88]
	Thermal stability	$LiNi_{0.915}Co_{0.075}Al_{0.01}O_2$	6.0–7.0	3.0–4.3	1.15 M $LiPF_6$ EC/DMC/EMC (1:2:2 v/v/v)	90.7%, 50th at 1C/1C		[89]
	Mitigating structural degradation	$LiCoO_2$		3.0–4.5	1 M $LiPF_6$ EC/EMC/DMC (1:1:1 v/v/v)	> 60.0%, 500th at 1C/1C		[115]
MoO_3	Mitigating structural degradation	$LiNi_{0.8}Co_{0.1}Mn_{0.1}O_2$	1.7	2.8–4.3	1 M $LiPF_6$ EC/EMC/DMC	94.8%, 100th at 1C/1C		[40]
MoO_3	Alleviating crack generation	$Li_{1.2}Mn_{0.56}Ni_{0.16}Co_{0.08}O_2$		2.0–4.8	(1:1:1 v/v/v)	91.5%, 100th at 1C/1C		[139]
Cr_2O_3		$LiNi_{0.8}Co_{0.15}Al_{0.05}O_2$		3.0–4.2	1 M $LiPF_6$ EC/DEC (1:1 w/w)	92.4%, 50th at 0.5C/0.5C		[116]
Nb_2O_5		$LiNi_{1/3}Co_{1/3}Mn_{1/3}O_2$	10.2	2.8–4.6	1 M $LiPF_6$ EC/DMC (3:7 v/v)	70.0%, 100th at 1C/1C		[125]
ZnO		$Li_{1.2}Mn_{0.54}Ni_{0.13}Co_{0.13}O_2$	2.5	2.0–4.8	1 M $LiPF_6$ EC/DMC (1:1 w/w)	97.5%, 100th at 0.2C/0.2C		[140]
ZnO		$LiNi_{0.8}Co_{0.15}Al_{0.05}O_2$	3.0	2.7–4.4	1 M $LiPF_6$ EC/DMC (1:1 v/v)	88.0%, 50th at 1C/1C		[149]
ZrO_2	Alleviating crack generation	$LiNi_{0.8}Co_{0.1}Mn_{0.1}O_2$	10.5	2.5–4.25	1 M $LiPF_6$ EC/DEC (1:1 v/v)	89.4%, 100th at 0.3C/0.3C		[150]
Al-Ti-oxide	Mitigating structural degradation	$LiCoO_2$		3.0–4.5	1 M $LiPF_6$ EC/PC/DMC/EMC/VC	96.9%, 100th at 1C/1C		[117]
AZO[a)]	Improving electronic conductivity	$LiCoO_2$		3.0–4.5	1 M $LiPF_6$ EC/DMC (1:1 v/v)	80.0%, 650th at 0.2C/0.2C	95.6 at 8C	[202]
$LiBO_2$	Mitigating structural degradation	$LiNi_{0.5}Co_{0.2}Mn_{0.3}O_2$	2.0	3.0–4.5	1 M $LiPF_6$ EC/EMC/DMC (1:1:1 v/v/v)	78.2%, 100th at 1C/1C		[118]
$LiBO_2$	Alleviating crack generation	$LiNi_{0.5}Co_{0.2}Mn_{0.3}O_2$		2.5–4.6	1 M $LiPF_6$ EC/DMC (1:2 v/v)	78.5%, 150th at 0.1C/0.1C		[151]
LBO[b)]	Alleviating crack generation Improving ion transport	$LiNi_{0.8}Co_{0.15}Al_{0.05}O_2$	4.2	2.75–4.3	1 M $LiPF_6$ EC/DEC/DMC (1:1:1 v/v/v)	85.2%, 200th at 2C/2C		[152]
		$LiNi_{0.8}Co_{0.15}Al_{0.05}O_2$ $LiCoO_2$		2.7–4.3	1 M $LiPF_6$ EC/EMC/DMC (1:1:1 v/v/v)	91.5%, 50th at 1C/1C	145.0 at 5C	[167]
LBO[b)]	Improving ion transport		1.5 mg cm^{-3}	3.0–4.5	1 M $LiPF_6$ EC/DEC/DMC (1:1:1 v/v/v)	84.4%, 100th at 1C/1C	95.0 at 10C	[169]
$LiCeO_2$	Enhancing oxygen redox							
		$Li_{1.2}Mn_{0.54}Ni_{0.13}Co_{0.13}O_2$		2.0–4.8	1 M $LiPF_6$ EC/DMC (1:1 v/v)	84.3%, 200th at 1C/1C		[157]
$LiTiO_2$	Improving ion transport	$LiNi_{0.815}Co_{0.15}Al_{0.035}O_2$	4.0–5.0	2.3–4.3	1 M $LiPF_6$ EC/EMC/DMC (1:1:1 v/v/v)	90.8%, 100th at 1C/1C	163.8 at 10C	[168]
Li_2TiO_3	Improving ion transport Mitigating structural degradation, Thermal stability	$LiNi_{0.8}Co_{0.15}Al_{0.05}O_2$	2.0	2.7–4.3	1 M $LiPF_6$ EC/DEC/DMC (1:1:1 v/v/v)	84.0%, 400th at 0.5C/0.5C	107.0 at 10C	[170]
Li_2TiO_3		$LiNi_{0.5}Co_{0.2}Mn_{0.3}O_2$	5.0	3.0–4.6	1 M $LiPF_6$ EC/DMC (1:1 w/w)	92.4%, 100th at 1C/1C		[119]
Li_2ZrO_3	Thermal stability, Improving ion transport	$LiNi_{0.8}Co_{0.1}Mn_{0.1}O_2$		2.8–4.5		83.2%, 200th at 1C/1C	164.7 at 10C	[43]
Li_2ZrO_3	Mitigating structural degradation	$LiCoO_2$	4.0	3.0–4.5	1 M $LiPF_6$ EC/DMC	85.2%, 100th at 5C/5C		[120]
Li_2CO_3	Alleviating crack generation	$LiNi_{0.7}Co_{0.15}Mn_{0.15}O_2$	4.0	3.0–4.5	1.2 M $LiPF_6$ EC/EMC (3:7)	92.8%, 100th at 0.33C/0.33C		[153]
	Improving ion transport	$LiNi_{0.6}Co_{0.2}Mn_{0.2}O_2$	3.7	2.8–4.6	1 M $LiPF_6$ EC/DMC (1:1 v/v)	85.5%, 100th at 0.2C/0.2C	157.9 at 10C	[171]
Li_2SiO_3	Improving ion transport	$Li_{1.2}Mn_{0.54}Ni_{0.13}Co_{0.13}O_2$	2.5	2.0–4.7		85.1%, 100th at 1C/1C	146.5 at 2C	[172]
Li_2SiO_3	Interfacial stabilization,	$Li_{1.13}Ni_{0.30}Mn_{0.57}O_2$		2.0–4.8	1 M $LiPF_6$ EC/DMC	67.3%, 300th at 1000 mA/g/1000 mA/g	123.0 at 400 mA/g	[173]
	Reducing oxygen redox	$Li_{1.2}Mn_{0.6}Ni_{0.2}O_2$	2.0	2.0–4.8		98.0%, 200th at 1C/1C		[158]
$LiAlO_2$	Improving ion transport	$Li(Li_{0.17}Ni_{0.2}Co_{0.05}Mn_{0.58})O_2$		2.0–4.8	1 M $LiPF_6$ EC/DMC (3:7 v/v)	91.3%, 70th at 5C/5C	144.5 at 5C	[174]
$LiAlO_2/LiCo_{1-x}Al_xO_2$	Mitigating structural degradation	$LiCoO_2$		3.0–4.5	1 M $LiPF_6$ EC/DEC/EMC (1:1:1 v/v/v)	73.0%, 500th at 1C/1C		[123]
$LiTaO_3$	Improving ion transport	$Li_{1.2}Ni_{0.17}Mn_{0.56}Co_{0.07}O_2$		2.0–4.8	1 M $LiPF_6$ EC/DMC (1:1 v/v)	80.3%, 200th at 0.1C/0.1C	172.4 at 3C	[30]
LLTO[c)]	Improving ion transport	$Li_{1.2}Ni_{0.2}Mn_{0.6}O_2$		2.0–4.8	1 M $LiPF_6$ EC/DEC (1:1 v/v)	86.5%, 100th at 1C/1C	114.1 at 5C	[175]
LLTO[c)]	Suppressing gas generation	$LiNi_{0.5}Co_{0.2}Mn_{0.3}O_2$		3.0–4.35	1 M $LiPF_6$ EC/DMC/EMC (3:3:4 v/v/v)	83.5%, 100th at 1C/1C		[105]

a) AZO: Aluminum doped zinc oxide, b) LBO: Lithium boron oxide, c) LLTO: Lithium lanthanum titanium oxide

reactions with HF to form fluoride compounds and H_2O, so they will later still face the original challenges because more water is generated during HF scavenging and this newly formed water can continue to hydrolyze $LiPF_6$ salt to generate new HF. Therefore, such scavenging method by using metal oxides as coating materials is not efficient although it may give protection to the cathode materials for a certain period of time.

Alternatively, inorganic phosphate compounds like Li_3PO_4 have been applied as a HF scavenger without generating extra H_2O. Jo et al. [75] suggested that the concentration of HF detected in the electrolyte after cycling was significantly reduced with a Li_3PO_4 coating layer on the surface of NCM622 cathode through the following manner:

$$Li_3PO_4 + HF \rightarrow Li_xH_yPO_4 \text{ (or } PO_xH_y) + LiF \quad (10)$$

The dissolved TM ions were also greatly decreased in Li_3PO_4-coated NCM622 benefiting from the reduced amount of HF in the electrolyte, which is well known to accelerate the gradual degradation of cathode active materials. Fig. 1a shows the HF titration and TM dissolution results for the electrolytes from the cells with bare and Li_3PO_4 coated NCM622 (1 wt.%) cathodes after 150 cycles. The concentration of HF was greatly reduced to 92 ppm for the coated cathode, compared to 239 ppm for the bare cathode. Due to the reduced HF in the electrolyte of Li_3PO_4-coated NCM622 cell, the amount of dissolved TM ions was also significantly decreased. For these reasons, the Li_3PO_4 coating layer led to good cycle performance, suppressed side reactions, and good structural stability, as shown in Fig. 1b.

Besides the replacement reaction with coating materials to consume HF, Lewis basicity of some polymers has also been utilized to scavenge HF. Kim et al. [76] developed a semi-interpenetrating polymer network (semi-IPN), which composes thermally stable cross-linked polyimide (PI) and polyvinylpyrrolidone (PVP), on the surface of $LiCoO_2$ (LCO) cathode materials. The PI/PVP coating layer exhibits significant HF-scavenging capability through the Lewis basic sites of pyrrolidone ring in PVP (Fig. 1c), as evidenced by the broadened X-ray photoelectron spectroscopy (XPS) peak corresponding to the nitrogen (N) atoms of pyrrolidone rings after the electrolyte absorption, which indicates the formation of N–H bonds. Such a chemically functional polymeric coating layer greatly improves the electrochemical performance. In addition, the contents of contaminated species (e.g. Li_2F^+) on the LCO surface and deposited Co compounds (presented by yellow dots in Fig. 1d) on the graphite anode surface after cycling are significantly decreased by suppressing the unwanted interfacial side reactions. Accordingly, surface modification strategies using HF-reactive metal oxides, phosphate compounds, and polymers including the Lewis basic sites have been successful in enhancing the cycle stability of TM layered oxide cathodes by mitigating the formation of acidic species.

Stabilizing cathode-electrolyte interphase

Some coating layers can act as an artificial cathode electrolyte interphase (CEI) on the surface of cathode materials to suppress electrolyte invasion and enhance the interfacial stability. Yim and coworkers [77] designed a sulfonate (SO_3)-based organic CEI layer on $LiNi_{0.8}Co_{0.1}Mn_{0.1}O_2$ (NCM811) cathode material. The CEI layer was synthesized by a quaternization reaction of sulfonate precursor, which was immobilized on the surface of cathode material by a wet-coating process. The developed SO_3-based CEI layer not only enhances the long-term cycling performance of NCM811 cathode but also improves the rate capability due to a suppression of undesired electrochemical reactions between NCM811 and electrolyte by the sulfonate functional groups (–S=O– and –S–O–) and the improved Li ion migration by the partially negative charges on the sulfonate functional groups that can bind with Li^+. According to a study by Son et al., [78] a uniform and thin artificial CEI layer (~10 nm) consisting of $LiCO_3R$ and Li_2CO_3 is conformally generated on $LiNi_{0.6}Co_{0.1}Mn_{0.3}O_2$ (NCM613) surface through a reaction with CO_2 and CH_4 mixed gas by a chemical vapor deposition (CVD) process in a self-limited manner. Benefiting from this gas phase coating, the artificial CEI layer has penetrated deep inside the core of each secondary particle as demonstrated by transmission electron microscopy (TEM) and energy dispersive X-ray spectroscopy (EDS) analysis (Fig. 2a and 2b). This artificial CEI layer exhibits superior interfacial stability in terms of greatly mitigated side reactions with electrolyte, and suppressed oxygen evolution, maintaining the structural stability during cycling. Thus, the artificial CEI coated NCM613 cathode shows improved battery performance at different cut-off voltages and temperature conditions (Fig. 2c) and clearly diminished metal-ion dissolution.

As for the LMR cathode materials, their high specific capacity of $\geq$280 mAh g^{-1} can only be achieved at voltages above 4.5 V (vs. Li/Li^+) after the electrochemical activation of monoclinic Li_2MnO_3. However, in this process, LMR cathode materials suffer from formidable challenges like low initial Coulombic efficiency (CE) and phase transition from layered to spinel, triggering voltage decay [7,79]. Furthermore, interfacial side reactions of LMR cathodes with liquid electrolytes severely occur, causing electrolyte decomposition and depletion as well as TM dissolution from LMR cathodes. Considering the continuous formation of spinel structure during the cycling of LMR at high voltages, researchers purposely generated a spinel layer on LMR particles to delay the fading of LMR cathodes. The preformed spinel layer, which is generated by the chemical removal of Li^+ from Li_2MnO_3, has a three-dimensional (3D) lattice structure. This 3D lattice structured spinel layer provides enhanced kinetics for Li^+ transport, correspondingly improving the CE during the first charge/discharge cycle. In addition, the preformed spinel layers prevent not only the interfacial side reactions between inner layered structure and electrolytes but also further phase transformations (layered to spinel) which cause structural disruption during cycling [80–82]. Liu et al. [83] coated CaF_2 on $Li_{1.2}Mn_{0.54}Ni_{0.13}Co_{0.13}O_2$, which results in enhanced cycling performance and reduced charge-transfer resistance. The CaF_2 coating layer seems to promote the formation of inactive O_2 molecules by accelerating phase transformation to spinel structure during coating process, thus it acts as a buffer layer between the cathode and the electrolyte, suppressing the degradation of the interface. It is indicated that such preformed spinel layers on LMR cathodes can improve the interfacial stability between the cathode and the electrolyte.

Moreover, the preformed spinel phase on LMR cathode surface can also be achieved by coating strategies involving a chemical extraction of Li ion from the LMR surface [84,85], or relying

TABLE 2

Summary of the surface modification using phosphates and fluorides.

Coating material	Function	Cathode active material	Mass loading [mg cm^{-2}]	Voltage range [V vs. Li/Li$^+$]	Electrolytes	Capacity retention after × cycles at charging/discharging C-rate	Capacity [mAh g^{-1}] at discharging C-rate	Ref.
Li_3PO_4	HF scavenging	$LiNi_{0.6}Co_{0.2}Mn_{0.2}O_2$		3.0–4.3	1 M $LiPF_6$ EC/DMC (3:7 v/v)	94.1%, 150th at 1C/1C	150.0 at 10C	[75]
	Improving ion transport		2.0–3.0	2.8–4.7	1 M $LiPF_6$ EC/DMC (1:1 v/v)	79.7%, 100th at 1C/1C		[92]
		$LiCoO_2$		3.0–4.5		79.3%, 100th at 1C/1C; 78.2%, 100th at 1C/1C (50 °C)		[93]
		$LiNi_{0.815}Co_{0.15}Al_{0.035}O_2$	4.5	2.75–4.3	1 M $LiPF_6$ EC/DEC (1:1 v/v)	92.7%, 100th at 0.5C/0.5C		[94]
	Alleviating crack generation	$LiNi_{0.76}Mn_{0.14}Co_{0.10}O_2$	4.0–5.0	2.7–4.5	1 M $LiPF_6$ EC/DMC (1:2 v/v)	91.6%, 200th at 0.33C/0.33C		[37]
		$LiNi_{0.8}Co_{0.1}Mn_{0.1}O_2$	1.9		1 M $LiPF_6$ EC/EMC (3:7 v/v)	85.0%, 200th at 0.33C/0.33C		[156]
	Alleviating crack generation, Inhibiting moisture/air exposure			2.5–4.3		96.0%, 100th at 95 mA/g/95 mA/g		[159]
	Inhibiting moisture/air exposure	$LiNi_{0.94}Co_{0.06}O_2$	1 mAh cm^{-2}		1 M $LiPF_6$ EC/EMC (3:7 v/v) +2wt.% VC	80.0%, 1000th at 0.5C/0.5C		[163]
	Improving ion transport	$LiNi_{0.8}Co_{0.1}Mn_{0.1}O_2$	2.0	3.0–4.4	1 M $LiPF_6$ EC/DEC/DMC	92.6%, 100th at 1C/1C	159.4 at 8C	[177]
		$Li(Li_{0.2}Mn_{0.54}Ni_{0.13}Co_{0.13})O_2$	3.5	2.0–4.8	(1:1:1 v/v/v)	85.0%, 100th at 0.5C/0.5C	129.1 at 2C	[185]
Li_3PO_4/C	Improving ion transport	$Li_{1.2}Ni_{0.13}Co_{0.13}Mn_{0.54}O_2$		2.0–4.6	1 M $LiPF_6$ EC/DMC (1:3 v/v)	75.1%, 200th at 0.5C/0.5C	98.5 at 33.3C	[176]
Li_3PO_4– CNT	Thermal stability, Inhibiting moisture/air exposure	$LiNi_{0.6}Co_{0.2}Mn_{0.2}O_2$		3.0–4.5		84.8%, 500th at 0.5C/0.5C		[96]
$MnPO_4$	Improving ion transport	$LiNi_{0.4}Co_{0.2}Mn_{0.4}O_2$	3.8–6.2	3.0–4.3	1 M $LiPF_6$ EC/DMC (1:1 v/v)	102.7%, 100th at 10C/10C	101.5 at 10C	[178]
		$LiNi_{0.6}Co_{0.2}Mn_{0.2}O_2$	1.8–2.2	3.0–4.6	1 M $LiPF_6$ EC/DMC (1:1 v/v) +1wt.% VC	70.7%, 50th at 10C/10C	114.5 at 10C	[179]
$LaPO_4$		$LiNi_{0.8}Co_{0.1}Mn_{0.1}O_2$		3.0–4.3		91.2%, 100th at 1C/1C	124.0 at 10C	[180]
YPO_4	Mitigating structural degradation	$LiNi_{0.88}Co_{0.09}Al_{0.03}O_2$	~2.0	2.7–4.5	1 M $LiPF_6$ EC/EMC/DMC (1:1:1 v/v/v)	88.9%, 100th at 1C/1C		[128]
$AlPO_4$	Thermal stability	$LiNi_{0.33}Co_{0.33}Mn_{0.33}O_2$	8.5	2.75–4.5	1 M $LiPF_6$ EC/EMC (3:7 v/v) +2wt.% VC	87.2%, 100th at 1C/1C		[95]
Al_2O_3–$AlPO_4$	Inhibiting moisture/air exposure	$LiNi_{0.5}Co_{0.2}Mn_{0.3}O_2$		3.0–4.6	1 M $LiPF_6$ EC/DMC (1:1 v/v)	95.5%, 50th at 0.2C/0.2C		[161]
Amorphous phosphate	Mitigating structural degradation	$LiNi_{0.8}Co_{0.15}Al_{0.05}O_2$		3.0–4.5		68.8%, 300th at 5C/5C		[127]
$Mn_3(PO_4)_2$	Thermal stability, Mitigating structural degradation	$LiNi_{0.6}Co_{0.2}Mn_{0.2}O_2$	1.1	3.0–4.3	1 M $LiPF_6$ EC/DMC (1:2 v/v)	92.6%, 50th at 0.5C/0.5C		[97]
$NaTi_2(PO_4)_3$	Improving ion transport		15.0	3.0–4.6	1 M $LiPF_6$ EC/EMC/DMC	85.3%, 100th at 0.5C/0.5C	165.6 at 10C	[181]
$LiZr_2(PO_4)_3$		$LiNi_{0.82}Co_{0.15}Al_{0.03}O_2$	3.0–4.0	2.7–4.3	(1:1:1 v/v/v)	84.6%, 100th at 1C/1C	151.7 at 5C	[182]
$Li_{1.3}Al_{0.3}Ti_{1.7}(PO_4)_3$		$Li_{1.2}Ni_{0.2}Mn_{0.6}O_2$		2.0–4.8	1 M $LiPF_6$ EC/DMC (1:1 v/v)	89.1%, 80th at 0.2C/0.2C	68.9 at 10C	[183]
LAGP[a)]	Mitigating structural degradation, Improving ion transport	$LiCoO_2$		3.0–4.5	1 M $LiPF_6$ EC/DEC (1:1 w/w)	91.8%, 300th at 0.3C/1C	163.0 at 6C	[124]
CaF_2	Interfacial stabilization	$Li_{1.2}Mn_{0.54}Ni_{0.13}Co_{0.13}O_2$	5.0–6.4	2.0–4.8	1 M $LiPF_6$ EC/DMC/DEC (1:1:1 v/v/v)	91.2%, 80th at 0.2C/0.2C		[83]
AlF_3	Thermal stability, Alleviating crack generation	$LiNi_{0.8}Co_{0.15}Al_{0.05}O_2$		2.7–4.3	1 M $LiPF_6$ EC/DEC (1:1 v/v)	86.2%, 1000th at 1C/1C		[90]
	Thermal stability	$Li(Li_{0.19}Ni_{0.16}Co_{0.08}Mn_{0.57})O_2$		2.0–4.6	1 M $LiPF_6$ EC/DMC (1:3 v/v)	91.6%, 100th at 0.5C/0.5C		[91]
	Thermal stability, Mitigating structural degradation	$Li(Li_{0.2}Ni_{0.17}Co_{0.07}Mn_{0.56})O_2$		2.0–4.8	1 M $LiPF_6$ EC/DMC (1:1 v/v)	83.1%, 50th at 0.1C/0.1C		[142]
	Mitigating structural degradation	$Li(Li_{0.17}Ni_{0.25}Mn_{0.58})O_2$			1 M $LiPF_6$ EC/DMC (3:7 v/v)	83.0%, 200th at 5C/5C		[144]
LiF		$Li_{1.2}Ni_{0.13}Co_{0.13}Mn_{0.54}O_2$			1 M $LiPF_6$ EC/DMC (1:1 v/v)	93.0%, 1000th at 10C/10C		[38]
$LiF/Li_xPF_yO_z$				2.0–4.6	1 M $LiPF_6$ EC/EMC/DMC (1:1:1 v/v/v)	91.2%,100th at 1000mAh/g /1000mAh/g		[143]
NaF			3.2	2.0–4.8	1 M $LiPF_6$ EC/DMC (1:1 v/v)	85.0%, 1000th at 10C/10C		[35]
$LiAlPO_{3.93}F_{1.07}$	Improving ionic/electronic conductivity	$LiCoO_2$		2.75–4.55	1 M $LiPF_6$ EC/DEC/EMC (1:1:1)	91.7%, 50th at 0.5C/0.5C	161.0 at 4C	[184]

a) LAGP: $Li_{1.5}Al_{0.5}Ge_{1.5}(PO_4)_3$.

TABLE 3

Summary of the surface modification using spinel, olivine, and layered active materials.

Coating material	Function	Cathode active material	Mass loading [mg cm^{-2}]	Voltage range [V vs. Li/Li$^+$]	Electrolytes	Capacity retention after × cycles at charging/discharging C-rate	Capacity [mAh g^{-1}] at discharging C-rate	Ref.
Spinel $Li_4Mn_5O_{12}$	Mitigating structural degradation, Thermal stability, Enhancing oxygen redox	$Li_{1.2}Mn_{0.54}Co_{0.13}Ni_{0.13}O_2$	3.0–5.0	2.0–4.7	1 M $LiPF_6$ EC/DMC/DEC (1:1:1 v/v/v)	83.1%, 300th at 0.2C/0.2C		[41]
Spinel $LiNi_{0.5}Mn_{1.5}O_4$-shell	Thermal stability, Alleviating crack generation	$LiNi_{0.88}Co_{0.09}Al_{0.03}O_2$	5.0–6.0	2.75–4.5	1 M $LiPF_6$ EC/DMC (1:1)	78.7%, 100th at 1C/1C		[50]
Spinel $LiNi_{0.5}Mn_{1.5}O_4$	Improving ion transport	$0.4Li_2MnO_3$·$0.6LiNi_{1/3}Co_{1/3}Mn_{1/3}O_2$	2.0–4.8			94.4%, 100th at 5C/5C	180.0 at 5C	[187]
Spinel $Li_xCo_2O_4$		$LiCoO_2$	3.0–4.5			85.4%, 50th at 0.5C/0.5C	137.0 at 3C	[188]
$Li_4Ti_5O_{12}$	Alleviating crack generation	Al-doped $LiCoO_2$	~12.0	2.8–4.5	1 M $LiPF_6$ EC/EMC (3:7 v/v) 2 wt.% VC 5 wt.% FEC	89.9%, 100th at 0.2C/0.2C		[154]
	Thermal stability	$LiNi_{0.5}Co_{0.2}Mn_{0.3}O_2$	3.0–4.5	3.0–4.5	1 M $LiPF_6$ EC/DMC/DEC (1:1:1 v/v/v)	91.0%, 100th at 0.5C/0.5C		[101]
	Improving ion transport	$LiNi_{0.6}Co_{0.1}Mn_{0.1}O_2$	2.7–4.3	2.7–4.3		85.8%, 40th at 5C/5C	106.3 at 10C	[189]
		$LiCoO_2$	3.0–4.5	3.0–4.5		90.0%, 60th at 0.2C/0.2C; 72.6%, 60th at 0.2C/0.2C (55 °C)	113.0 at 12C	[191]
$LiFePO_4$	Thermal stability, Mitigating structural degradation	$LiNi_{0.8}Co_{0.15}Al_{0.05}O_2$		2.8–4.3		89.4%, 200th at 2C/2C		[102]
				2.75–4.5		95.0%, 100th at 0.5C/0.5C		[103]
$Li_3V_2(PO_4)_3$ (LVP)	Improving ion transport	$Li_{1.17}Ni_{0.2}Co_{0.03}Mn_{0.58}O_2$		2.0–4.8		94.4%, 100th at 5C/5C	162.8 at 5C	[186]
Spinel (Co_3O_4–Li_xCoO_2) Layered $LiCoO_2$ nanostructured stabilizer	Mitigating structural degradation, Thermal stability	$LiNi_{0.8}Co_{0.1}Mn_{0.1}O_2$	~12.0	3.0–4.3	1 M $LiPF_6$ EC/EMC/DMC (3:6:1 v/v/v) 1 wt.% VC 0.5 wt.% 1,3- propane sultone	49.3%, 500th at 0.5C/1.0C (45 °C)		[26]
$LiCoO_2$ glue layer	Alleviating crack generation, Improving ion transport	$LiNi_{0.8}Co_{0.15}Al_{0.05}O_2$	~8.0		1.15 M $LiPF_6$ EC/DMC/DEC(3:4:3 v/v/v)	87.0%, 300th at 0.5C/1.0C	147.0 at 7C	[155]

on an acid treatment of LMR to allow an ion-exchange reaction between Li^+ and H^+ [86,87]. Song et al. [84] studied graphene oxide (GO) wrapped $Li_{1.2}Mn_{0.54}Ni_{0.13}Co_{0.13}O_2$ (LLNCM) with L-ascorbic acid (LAA) aqueous solution immersion and heat treatment to generate a graphene-spinel double protecting layer on the surface of LLNCM cathode material. The acidic environment provided by GO and LAA results in some ion exchanges between Li^+ and H^+ ions, and the removal of H^+ ions from the surface during heating process leads to the formation of both reduced GO (rGO) and vacancies and consequently the thermodynamically stable spinel phase. Besides, rGO may lead to the reduction of TM ions with high oxidation states during the heating process and such reduction effects also contribute to spinel formation on the surface of LLNCM. The newly formed spinel surface as an interfacial protective layer effectively suppresses further phase transition in LLNCM upon cycling. In a similar way, rGO coating $0.4Li_2MnO_3$-$0.6LiNi_{1/3}Co_{1/3}Mn_{1/3}O_2$ (HGO) by sol–gel process with hydrazine solution was also proposed [85]. It is demonstrated by high-resolution TEM (HR-TEM) that not only ~1.14 nm of rGO layer but also ~3 nm of chemically activated layer are formed on the cathode surface by this modification (Fig. 2d). Fig. 2e shows that rGO coated cathode produces improved initial CE by the stabilization effects. As shown in Fig. 2f, the combination of the thin rGO coating layer and the activated layer via the chemical treatment effectively enhances the surface electronic conductivity, suppresses the side reactions, and maintains structural stability during the cycling for HGO cathode. These results prove that forming a thin spinel layer on LMR surface through surface modification with ion-exchange can provide interfacial stability to LMR cathodes. However, caution should be paid to avoid the possibility that acid treatment may cause a structural disruption of the LMR cathode, resulting in subsequent loss of electrochemical sustainability. Artificial CEI layers are mostly generated by the interfacial reaction between the coating material and the elements on the surface of cathodes. The stabilized surface of layered TM oxides cathodes benefiting by an artificial CEI layer can not only inhibit undesirable side reactions but also prevent structural degradation from spreading to the inner layered structure.

Enhancing thermal stability

Layered TM oxide cathode materials have safety concerns resulting from thermal runaway especially at the charged state because of structural instability and electrolyte decomposition. In terms of controlling the surface of the cathode, coating strategy has been considered as an effective way to provide thermal stability. Among a variety of candidate materials [88–97], metal phosphates [92–97] have been preferred because of their strong P–O bonding. Ming and coworkers [95] introduced a uniform and ultrathin $AlPO_4$ coating layer on the surface of $LiNi_{1/3}Co_{1/3}Mn_{1/3}O_2$ (NCM111) cathode material via an *in-situ* coating approach based on an organic ligand coordination complex. The coating layer delivers an extraordinary anticorrosive and antioxidation capability which benefits from the strong covalent bond between Al^{3+} and PO_4^{3-}, enabling superior thermal stability in the cells with $AlPO_4$ coated NCM111 cathode as confirmed by both overcharge experiment (Fig. 3a) and high-temperature storage performance (Fig. 3b). As shown in Fig. 3a, during overcharge

TABLE 4

Summary of the surface modification using organic materials and some special surface treatments.

Coating material	Function	Cathode active material	Mass loading [mg cm^{-2}]	Voltage range [V vs. Li/Li$^+$]	Electrolytes	Capacity retention after × cycles at charging/discharging C-rate	Capacity [mAh g^{-1}] at discharging C-rate	Ref.
Polyimide	Thermal stability	$LiNi_{1/3}Co_{1/3}Mn_{1/3}O_2$		2.8–4.8	1 M $LiPF_6$ EC/DMC (1:1 v/v)	66.0%, 50th at 1C/1C		[98]
		$LiCoO_2$		3.0–4.4	1 M $LiPF_6$ EC/EMC (1:2 v/v)	85.0%, 50th at 0.5C/0.5C		[99]
		$Li_{1.2}Ni_{0.13}Mn_{0.54}Co_{0.13}O_2$		2.0–4.8	1 M $LiPF_6$ EC/DMC (1:1 v/v)	90.6%, 50th at 0.1C/0.1C		[100]
PI/PVP[a)]	HF scavenging, Thermal stability	$LiCoO_2$	16.0	3.0–4.4	1 M $LiPF_6$ EC/EMC (1:2 v/v)	85.0%, 80th at 0.5C/0.5C		[76]
PDMS[b)] (–OH)	Inhibiting moisture/air exposure	$LiNi_{0.8}Co_{0.1}Mn_{0.1}O_2$	2.2–2.4		1 M $LiPF_6$ EC/EMC/DMC (3:4:3 v/v/v)	75.3%, 200th at 0.5C/0.5C		[164]
OPA[c)]			~4.0	2.8–4.3	1 M $LiPF_6$ EC/DMC/EMC	74.3%, 197th at 0.5C/0.5C		[165]
PMMA	Improving ionic conductivity		4.5–5.1		(1:1:1 v/v/v)	91.2%, 100th at 1C/1C	157.8 at 20C	[193]
PANI[d)]	Improving electronic conductivity	$Li(Li_{0.2}Mn_{0.54}Ni_{0.13}Co_{0.13})O_2$		2.0–4.8	1 M $LiPF_6$ EC/DMC (1:1 v/v)		198.6 at 10C	[194]
PANI-PVP[e)]	Improving ionic/electronic conductivity	$LiNi_{0.8}Co_{0.1}Mn_{0.1}O_2$	4.4–4.6	2.8–4.3	1 M $LiPF_6$ EC/DMC/EMC (1:1:1 v/v/v)	88.7%, 100th at 200mAh/g/200mAh/g	152.0 at 1000 mAh/g	[44]
PANI-PEG[f)]			4.0		1 M $LiPF_6$ EC/DMC/DEC (1:1:1 v/v/v)	92.4%, 100th at 1C/1C; 81.4%, 100th at 1C/1C (55 °C)	156.7 at 10C	[195]
PEDOT[g)]	Thermal stability,	$LiNi_{1/3}Co_{1/3}Mn_{1/3}O_2$		3.0–4.6	1 M $LiPF_6$ EC/EMC (3:7 v/v)	91.1%, 200th at 1C/1C		[45]
	Alleviating crack generation,	$LiNi_{0.85}Co_{0.1}Mn_{0.05}O_2$		2.7–4.3		91.0%, 100th at 1C/1C		
	Mitigating structural degradation	$Li_{1.2}Mn_{0.54}Ni_{0.13}Co_{0.13}O_2$		2.0–4.8		93.0%, 100th at 0.1C/0.1C		
PEDOT:PSS[h)]	Improving electronic conductivity	$Li_{1.2}Ni_{0.2}Mn_{0.6}O_2$			1 M $LiPF_6$ EC/DMC (1:1 v/v)	51.6%, 100th at 1C/1C	146.9 at 2C	[203]
NPPy[i)]	Mitigating structural degradation	$Li_{1.4}Mn_{0.6}Ni_{0.2}Co_{0.2}O_{2.4}$		2.0–4.6		89.0%, 200th at 0.5C/0.5C		[146]
Li_3PO_4–PPy[j)]	Improving ionic/electronic conductivity	$LiNi_{0.8}Co_{0.1}Mn_{0.1}O_2$		2.8–4.5		86.5%, 200th at 1C/1C	159.7 at 10C	[46]
rGO[k)]	Improving electronic conductivity	$LiNi_{0.6}Co_{0.2}Mn_{0.2}O_2$		3.0–4.6	1.15 M $LiPF_6$ EC/DMC/DEC (3:4:3 v/v/v)	98.1%, 100th at 0.1C/0.1C	132.6 at 10C	[196]
	Improving ionic/electronic conductivity	$LiNi_{0.815}Co_{0.15}Al_{0.035}O_2$		2.75–4.3	1 M $LiPF_6$ EC/DMC/DEC (1:1:1 v/v/v)	91.7%, 100th at 1C/1C	127.0 at 5C	[197]
rGO–LAA[l)]	Interfacial stabilization, Thermal stability Improving electronic conductivity	$Li_{1.2}Mn_{0.54}Ni_{0.13}Co_{0.13}O_2$	4.0–5.0	2.0–4.8	1 M $LiPF_6$ EC/DEC (1:1)		125.0 at 10C	[84]
rGO-hydrazine	Interfacial stabilization, Improving electronic conductivity	$0.4Li_2MnO_3{\cdot}0.6LiNi_{1/3}Mn_{1/3}Co_{1/3}O_2$	4.0–4.2	2.0–4.6	1.15 M $LiPF_6$ EC/DMC/DEC (3:4:3 v/v/v)	78.0%, 100th at 0.1C/0.1C	160 at 12C	[85]
rGO-KH560 polymer composite layer	Thermal stability, Improving electronic conductivity	$LiNi_{0.8}Co_{0.1}Mn_{0.1}O_2$		3.0–4.5	1 M $LiPF_6$ EC/DEC/equilibrium moisture content (1:1:1 v/v/v)	95.2%, 150th at 1C/1C	140.6 at 1C	[198]
Grephene	Improving electronic conductivity	$LiNi_{0.8}Co_{0.15}Al_{0.05}O_2$		2.8–4.3	1.2 M $LiPF_6$ EC/DEC/EMC (1:1:1 v/v/v)	82.1%, 100th at 5C/5C	153.6 at 5C	[199]
Porous active carbon		$LiNi_{1/3}Co_{1/3}Mn_{1/3}O_2$	5.0	2.5–4.5	1 M $LiPF_6$ EC/DMC (1:1 v/v)	90.3%, 100th at 1C/1C	54.6 at 40C	[200]
Carbon fiber		$LiNi_{0.88}Co_{0.06}Mn_{0.06}O_2$	2.0	2.8–4.3	1.2 M $LiPF_6$ EC/EMC (3:7)	67.3%, 150th at 0.5C/0.5C	137 at 10C	[201]
SO_3	Interfacial stabilization	$LiNi_{0.8}Co_{0.1}Mn_{0.1}O_2$	9.5	3.0–4.3	1 M $LiPF_6$ EC/EMC (1:2)	97.4%, 50th at 1C/1C		[77]
CVD with mixed CO_2/CH_4 gases		$LiNi_{0.6}Co_{0.1}Mn_{0.3}O_2$	5.4–16.2	2.5–4.5	1.3 M $LiPF_6$ EC/DEC/FEC (2:6:2 v/v/v)	99.5%, 100th at 1C/1C		[78]
0.1 M H_2SO_4	Suppressing gas generation	$Li_{1.16}Ni_{0.20}Co_{0.20}Mn_{0.44}O_2$		2.5–4.8	1 M $LiPF_6$ EC/DEC (3:7)	80.0%, 100th at 0.2C/0.2C		[106]
TMA[m)]		$0.35Li_2MnO_3{\cdot}0.65LiNi_{0.35}Mn_{0.45}Co_{0.20}O_2$		2.0–4.7				[61] [107]
Soaking in H_2O		$LiNi_{0.6}Co_{0.2}Mn_{0.2}O_2$		2.8–4.8	1 M $LiPF_6$ EC/DEC			[59]

a) PI/PVP: Polyimide-Polypyrrolidone, b) PMDS: Polydimethylsiloxane, c) OPA: Octadecylphosphonic acid, d) PANI: Polyaniline, e) PANI-PVP: Polyaniline-Polypyrrolidone, f) PANI-PEG: Polyaniline-Polyethylene glycol, g) PEDOT: poly(3,4-ethylene-dioxythiophene), h) PSS: polystyrene sulfonate, i) NPPy: Naphthalene sulfonic acid-doped polypyrrole, j) PPy: Polypyrrole, k) rGO: reduced graphene oxide, l) L-ascorbic acid: LAA , m) TMA: trimethylaluminum.

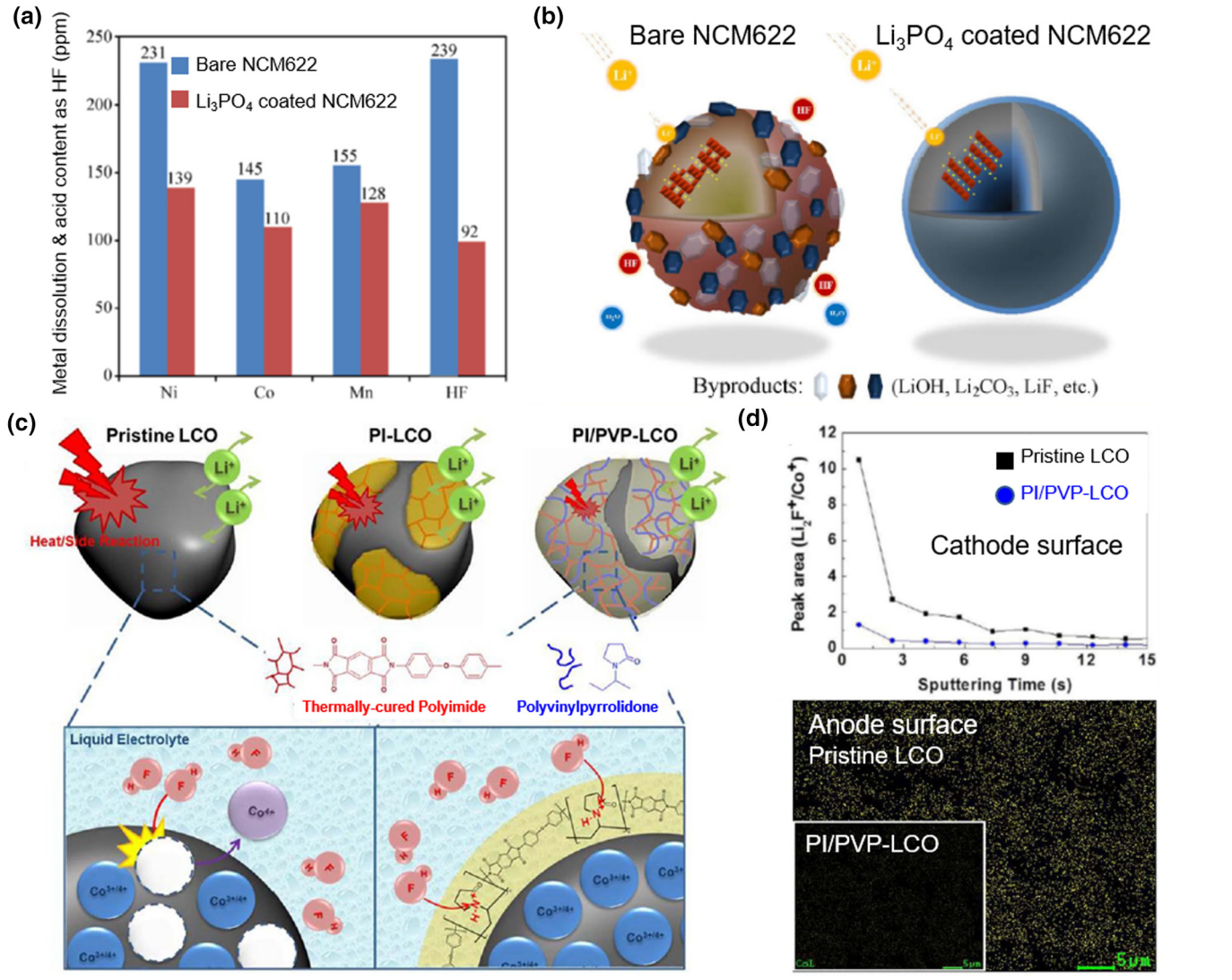

FIGURE 1

(a) HF titration and TM dissolution results for the electrolytes from the cells using bare and Li_3PO_4 coated NCM622 after cycling; (b) Schematic illustration of byproducts on the surfaces of bare and Li_3PO_4 coated NCM622 after cycling. Reproduced with permission [75]. Copyright 2015, Springer Nature. (c) A conceptual illustration depicting multifunctional benefits of PI/PVP nanoencapsulating layer on the interfacial stability between delithiated LCO and liquid electrolyte; (d) TOF-SIMS depth profile (up) of Li_2F^+ concentration on LCO surface and EDS images (down) showing Co elements (represented by yellow dots) deposited on anode surface for a cell incorporating pristine LCO (inset image is for PI/PVP-LCO) after 80 cycles. Reproduced with permission [76]. Copyright 2014, Springer Nature.

to 10.0 V of 1.0 Ah pouch cells, the cell with $AlPO_4$ coated NCM111 exhibits a temperature of ~36 °C at 5.5 V, while the cell with pristine NCM111 shows severe thermal runaway at 5.06 V with a sharply increased temperature of 90 °C within a few seconds. In Fig. 3b, during the storage of the batteries at fully charged state under 100 °C, the battery with the coated cathode presents a much suppressed voltage decay with the battery voltage maintained at 4.0 V for 6 days, but the voltage value drops to 3.93 V for the battery with the pristine NCM111 (Fig. 3b). Moreover, the $AlPO_4$ coating significantly enhances the cell performance of NCM111 at high voltage with preserved structural stability.

As a thermally stable organic material, PI has been introduced onto the surfaces of several cathode materials via *in situ* thermal imidization of the related precursors [98–100]. Park et al. [98] studied the thermal behavior of NCM111 cathode coated with a thermally cross-linked PI thin layer. As observed in differential scanning calorimetry (DSC) thermograms, PI coated NCM111 shows a noticeable reduction in the total amount of heat generation and a higher exothermic peak temperature when compared to the pristine NCM111 during charging to 4.6 and 4.8 V. The DSC results indicate the thermally stabilized interface between the cathode and liquid electrolyte in PI-coated NCM111 cathode, which should be ascribed to the effective protection enabled by the highly wrapped PI layer on the cathode surface. In addition, the PI coating layer can provide the coated cathode a high ionic conductivity of 0.15 mS cm^{-1} when swelling with the carbonate liquid electrolyte. Consequently, the chemically stable PI-coated NCM111 cathode delivers an improved capacity retention even with a 4.8 V cut-off voltage.

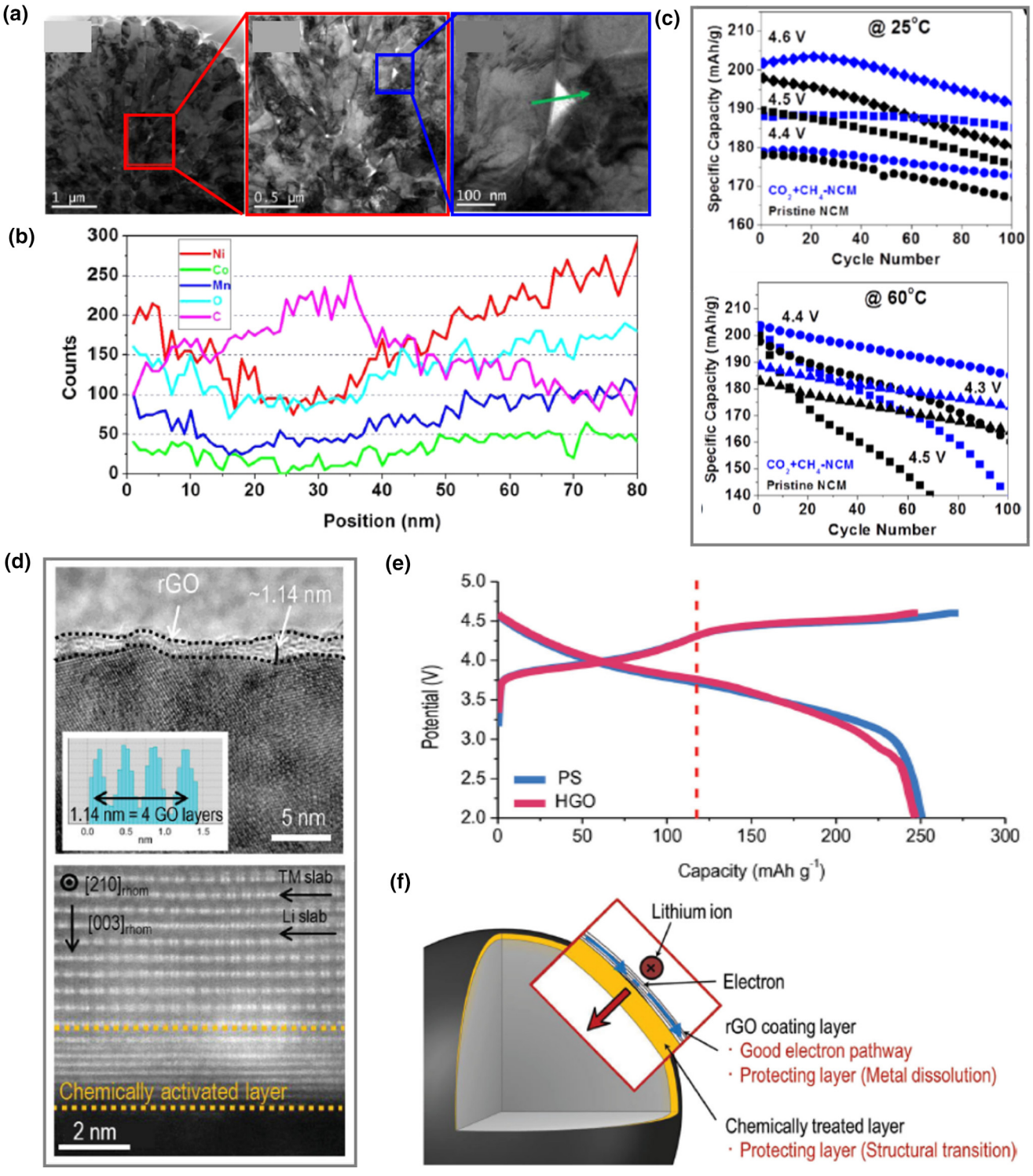

FIGURE 2

(a) TEM images and (b) EDS analysis of $CO_2 + CH_4$ coated NCM613. The green arrow in TEM images indicates the direction of EDS scan; (c) the discharge capacity retentions of the pristine and $CO_2 + CH_4$ coated NCM613 with different upper cutoff voltages at 25 and 60 °C, respectively. Reproduced with permission [78]. Copyright 2015, American Chemical Society. (d) HR-TEM images of the rGO coated sample (up) and HAADF-STEM images of hydrazine treated sample (down); (e) Voltage profiles of pristine (PS) and HGO cathodes in coin-type half cells between 2.0 and 4.6 V at 0.1C rate; (f) Schematic views of coated surface morphologies constructing hybrid surface layers consisting of rGO and chemically activated phase. Reproduced with permission [85]. Copyright 2014, Wiley-VCH.

On the other hand, spinel [41,50,101] and olivine [102,103] electrode materials, such as $Li_4Mn_5O_{12}$, $Li_4Ti_5O_{12}$, and $LiFePO_4$ (LFP), which possess relatively better thermal stability than layered cathodes, were also selected as coating materials [104]. Zhang et al. [41] reported a hetero-structured spinel $Li_4Mn_5O_{12}$-coated $Li_{1.2}Mn_{0.54}Co_{0.13}Ni_{0.13}O_2$ cathode (HETE). The HETE

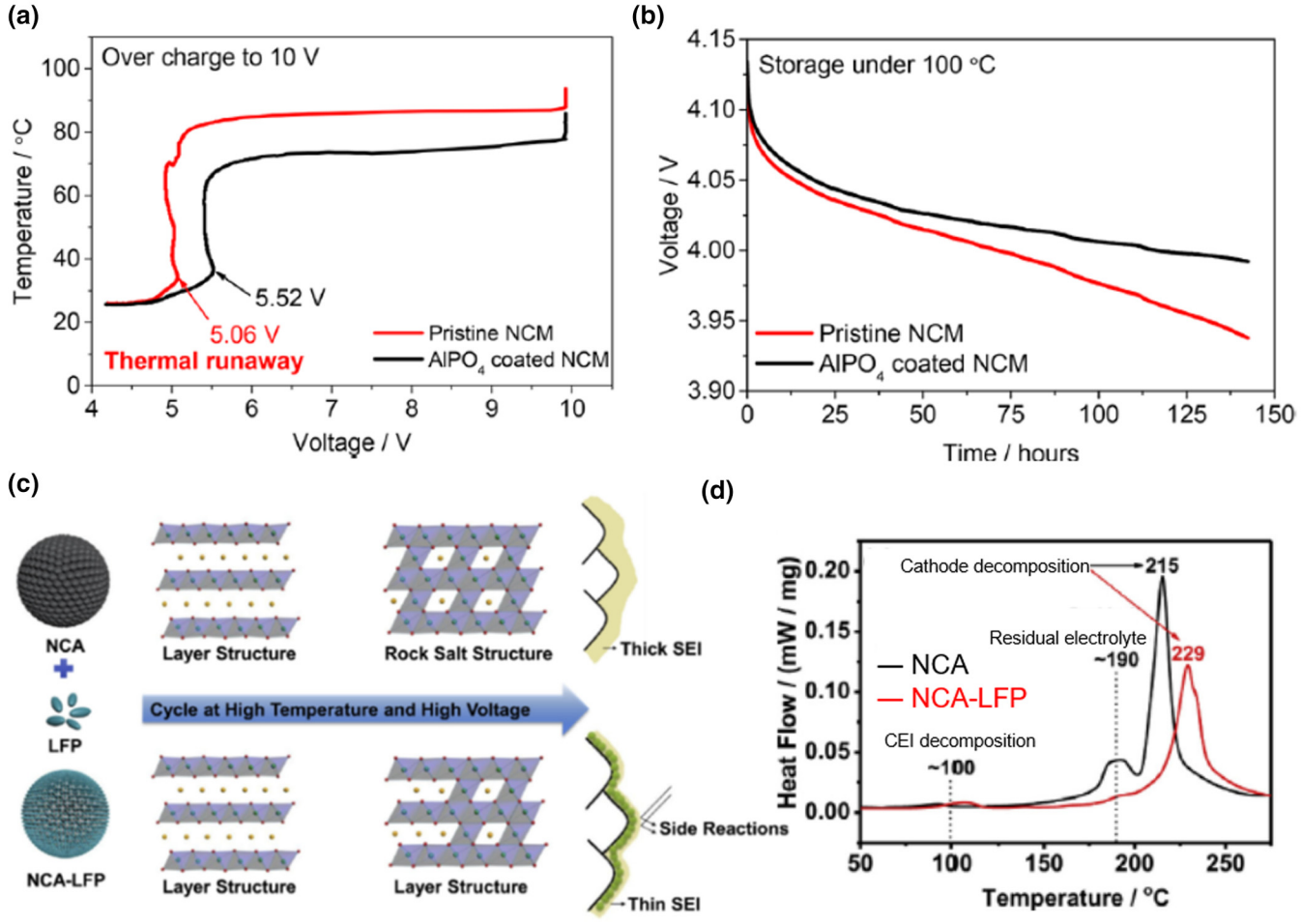

FIGURE 3

Comparison of the anti-overcharge and high-temperature storage performance of pristine and $AlPO_4$ coated NCM111: (a) temperature vs. voltage curves of the pouch cells and (b) self-discharge performance where the batteries were stored under 100 °C at the fully charged state. Reproduced with permission [95]. Copyright 2019, American Chemical Society. (c) A scheme illustrating the effects of LFP coating layers on NCA cathodes; (d) DSC exothermic peaks at a fully delithiated NCA cathode (4.2 V). Reproduced with permission [103]. Copyright 2019, Elsevier.

shows improved safety as demonstrated by the higher onset temperature than the pristine sample in the DSC testing of delithiated samples. Moreover, the $Li_4Mn_5O_{12}$ coating could alleviate the undesirable phase transformation and suppress the increment of charge transfer due to its thermodynamic stability. Thus, the spinel phase surface provides an enhancement in cycling performance even at 55 °C. LFP coating is also an effective method to enhance safety because of its high thermal and chemical stability. In the work of Chen et al. [103], the NCA cathode coated with LFP nanoparticles gives excellent cell performance including higher initial capacity and capacity retention after cycling due to the formation of a thinner CEI layer (Fig. 3c), which could be attributed to the mitigated electrolyte decomposition on the surface of LFP-coated NCA at higher charging voltage. This thin CEI layer can not only effectively preserve the layered structure but also reduce side reactions, resulting in a shifted exothermic peak to higher temperatures at charged state in the DSC measurement (Fig. 3d). According to the aforementioned results, when the intrinsically thermally stable materials, such as phosphates, polyimides, spinels, and olivine metal oxides, are applied as coating materials, it could accordingly allow improved thermal stability on the surface of the cathode.

Suppressing gas generation

Residual Li compounds, such as Li_2CO_3 and LiOH, on the surface of layered TM oxide cathodes give rise to gas evolution by electrochemically oxidized reactions and chemical reactions as shown below, which causes a series of safety issues.

$$2Li_2CO_3 \rightarrow 4Li^+ + 4e^- + 2CO_2\uparrow + O_2\uparrow \quad (11)$$

$$Li_2CO_3 + 2HF \rightarrow 2CO_2\uparrow + H_2O + 2LiF \quad (12)$$

$$C_3H_6O_3(\text{carbonate}) + Li_2CO_3 + 2HF \rightarrow C_3H_5O_3Li + CO_2\uparrow + H_2O + LiF \quad (13)$$

$$4LiOH \rightarrow 4Li^+ + 4e^- + 2H_2O + O_2\uparrow \quad (14)$$

Therefore, preventing the contact of the cathode with the electrolyte is a straightforward approach to suppress gas generation. At this point, surface modification, which can remove resid-

ual Li compounds or suppress TM–O bond cleavage during charging, is suggested as a very effective way for mitigating gas generation. It is reported that covering the surface of $LiNi_{0.5}Co_{0.2}Mn_{0.3}O_2$ (NCM523) cathode by lithium lanthanum titanium oxide (LLTO) [105] can suppress gas release during storage under 85 °C even on charging at 4.45 V. Another simple way is to reduce the amount of Li_2CO_3 and LiOH on the cathode surface. McCloskey and coworkers [59] studied the effect of soaking or washing NCM622 in water on outgassing under high charging voltage (>4.4 V). In that work, by soaking in water, which can remove the Li_2CO_3 and LiOH species and allow partial delithiation of the lattices, the treated NCM622 shows the lowest gas evolution during a 4.8 V hold (Fig. 4a). This result indicates that reducing residual Li species on the surface of cathode can effectively prevent electrolyte reactivity, leading to decreased gas evolution. However, soaking or washing layered oxide cathodes in water carries a risk of being harmful to sustain electrochemical performances, especially for Ni-rich layered TM oxide cathodes, such as NCM622 and NCM811. Recently Zhang et al. [106] reported a simple approach to remove residual Li species like Li_2O, LiOH and Li_2CO_3 formed on NCM811 particle surfaces during material storage by ball milling the NCM811 powder with a small amount of $LiPF_6$ (0.5–1.0 wt.%) in N-Methyl-2-pyrrolidone (NMP) solvent. During the milling process, these residual Li species on the cathode surface would react with the acidic $LiPF_6$ to form Li_3PO_4, LiF and/or H_2O, and CO_2 through the following reactions.

$$LiPF_6 + 4\ Li_2O \rightarrow Li_3PO_4 + 6\ LiF \quad (15)$$

$$LiPF_6 + 8\ LiOH \rightarrow Li_3PO_4 + 6\ LiF + 4\ H_2O \quad (16)$$

$$LiPF_6 + 4\ Li_2CO_3 \rightarrow Li_3PO_4 + 6\ LiF + 4\ CO_2 \uparrow \quad (17)$$

Since Li_3PO_4 and LiF are scarcely dissolved in NMP, they would precipitate and cover the NCM811 particle surface as a coating layer, while the H_2O and CO_2 would be removed during the filtration or milling processes. It has been reported that Li_3PO_4 and LiF are favorable to build a robust CEI on cathodes [107,108]. Therefore, the obtained NCM811 gave improved cycling stability and rate capacity after this simple pretreatment.

LMR cathode materials which consist of Li_2MnO_3 and layered TM oxides release O_2 gas during not only the initial cycle by electrochemical activation but also the oxygen redox reaction in the subsequent cycling. As mentioned in Section of Stabilizing cathode-electrolyte interphase, the acid treatment for LMR cathodes can induce Li^+ extraction by ion exchange. It is demonstrated by McCloskey and coworkers that the surface treatment of $Li_{1.16}Ni_{0.20}Co_{0.20}Mn_{0.44}O_2$ with 0.1 M H_2SO_4 not only provides chemical removal of Li^+ from Li_2MnO_3 and a partial reduction of Mn (Mn^{4+} to Mn^{3+}), but also removes ~58% of the residual Li_2CO_3 on the surface of the cathode particles, resulting in a substantial suppression of CO_2 (~92%) and O_2 (~100%) evolution during the first charge up to 4.8 V [109]. More importantly, the acid treatment effectively suppresses O_2 release occurring from oxide anion oxidation at the cathode surface without destroying the reversibility of oxygen redox in the particle bulk. Consequently, the acid treated LMR shows improved

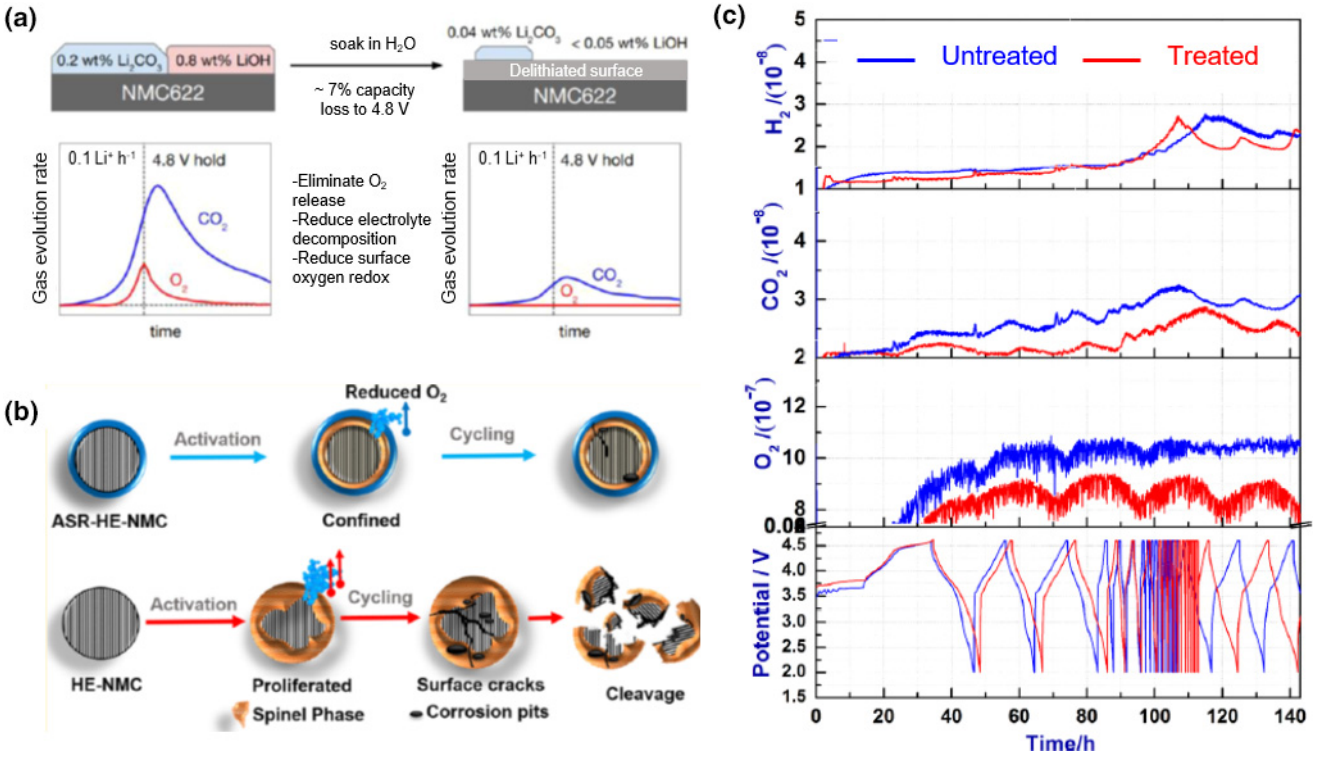

FIGURE 4

(a) Schematic illustration of soaking effect on gas evolution during the 4.8 V hold [59]. Copy right 2019, American Chemical Society. (b) Schematic illustration of ASR treatment by TMA to maintain $0.35Li_2MnO_3{\cdot}0.65LiNi_{0.35}Mn_{0.45}Co_{0.20}O_2$ particle; (c) comparative in-operando OEMS analysis of H_2, CO_2 and O_2 evolved as a function of applied potential during galvanostatic cycling. Reproduced with permission [61]. Copyright 2019, American Chemical Society.

rate and long-term cycling performance with small overpotential regarding interfacial reaction.

Interfacial atomic surface reduction (ASR) has been reported to be an effective approach to alter the electronic structure of cathode surface, resulting in a surface layer with reduced TM valance. In the studies by Noked and coworkers [61,110], ASR with trimethyl aluminum (TMA) as a volatile reducing agent was utilized to treat $0.35Li_2MnO_3{\cdot}0.65LiNi_{0.35}Mn_{0.45}Co_{0.20}O_2$ for the purpose of protecting structure and reducing oxygen evolution (Fig. 4b). Density functional theory (DFT) calculation demonstrated that the TMA molecules can bond onto both TM cations and O anions, resulting in improved surface stability [110]. The ASR treatment leads to a highly uniform ~3 nm thick amorphous layer composed of an altered electronic structure of Mn and Ni on the surface of the cathode. These are speculated to be responsible for the suppression of TM–O bond cleavage during charging, consequently resulting in lower O_2 evolution as indicated in the online electrochemical mass spectrometry (OEMS) curves in Fig. 4c. The ASR treated surface can also act as a buffer layer to delay the exposure to electrolyte and thus to suppress the parasitic reactions, which can be clearly evidenced from lower CO_2 and H_2 evolutions in Fig. 4c. The higher stability and reduced parasitic reactions in ASR treated cathode enable significant improvement in battery performance, including enhanced capacity and rate capabilities, narrowed voltage hysteresis, and doubled Li^+ diffusion ability [61]. These results present that reduced TM valance on the surface of cathode without introducing foreign materials will be a promising solution to alleviate gas generation.

In addition, spinel $Li_4Mn_5O_{12}$ coating, which can be achieved by a controlled oxidation of TM ions (principally Mn) near the surface of LMR cathodes by $KMnO_4$, followed by transformation to a spinel phase driven by the higher thermodynamic stability of the Mn-based spinel structure, has been reported to be effective in suppressing oxygen release [41]. The uniform covering of the heterostructured $Li_4Mn_5O_{12}$ layer is demonstrated to be inherently stable in the lattice framework to prevent oxygen release from $Li_{1.2}Mn_{0.54}Co_{0.13}Ni_{0.13}O_2$ at the deep delithiated state, leading to the superior cycling stability, good voltage stability, and favorable kinetics of spinel $Li_4Mn_5O_{12}$ coating cathode.

Strategies for alleviating instability at high voltages

Mitigating structural degradation

In general, a higher charge cut-off voltage allows layered TM oxide cathodes, such as LCO, $LiNi_xCo_yMn_{1-x-y}O_2$ (NCM), and NCA to deliver a higher specific capacity because of the increased amount of deintercalated Li ion [7,104,111]. However, most of the cathode materials suffer structural instability including phase transition due to the large amount of Li ion vacancies [66,69]. To address the unavoidable challenges of structural instability at high voltages, various strategies such as coating, doping, core–shell, and concentration-gradient have been reported [112–133]. In this subsection, we focus on coating strategies, which have been demonstrated to be effective in overcoming these formidable issues for LMO and LMR cathode materials.

LCO has been a promising cathode because of the high theoretical capacity of 274 mAh g^{-1}, while this is hard to reach due to the chemical instability of Li_xCoO_2 when more than 0.5 Li ion per unit (>4.2 V vs Li/Li^+) is deintercalated during the charging process. The chemical instability is due to the overlap of the $Co^{3+/4+}$:3d band with the top of the O^{2-}:2p band, removal of electron density from the band, and the consequent release of oxygen from the lattice [134,135]. TiO_2 has been considered as an effective coating material, which inhibits the structural degradation of LCO after charging because some Ti atoms could diffuse into the bulk of LCO, enabling the formation of a solid-state phase $LiTi_yCo_{1-y}O_{2+0.5y}$ during the heating process [121,122]. Wang et al. [121] reported that TiO_2 coating reduces the activity of 2-coordinated oxygen and increases the oxygen vacancy formation energy on the surface of TiO_2 coated LCO, which are mainly because Ti can donate more electrons than Co. Therefore, the TiO_2-coated LCO can delay the phase transformation from layer structure to spinel or rock-salt phase in the surface of LCO during cycling. Further, Zhou et al. [122] demonstrated the structural stability of TiO_2-coated LCO by comparing the X-ray diffraction (XRD) patterns after 50 cycles. The cycled bare LCO presents a broadened (003) peak while the (003) peak for the TiO_2-coated LCO exhibits a relatively high intensity. Deep Li ion extraction from LCO beyond 50% may form O vacancies especially on the surface, resulting in parts of the phase change to spinel or rock-salt.

In another effort, a $LiAlO_2$–$LiCo_{1-x}Al_xO_2$ double-layer, which has a hexagonal structure like LCO, was applied as a protective material to inhibit structural change [123]. In this double-layer, $LiCo_{1-x}Al_xO_2$ is easily combined with the surface of LCO through solid-state diffusion during thermal treatment. The increase of c-axis length in double-layer coated LCO was observed to be lower than that of Al_2O_3 single-layer-coated LCO after 500 cycles. This is because $LiCo_{1-x}Al_xO_2$ supplies not only suppressed phase transformation through preserving the Li ion content in the lattice but also high Li ion conductivity, which are different from the electrochemically insulating Al_2O_3. In addition, chemically inert $LiAlO_2$ layer isolates the direct contact between LCO and electrolyte. Therefore, the double-layer-coated LCO delivers much improved cycling stability compared with the single-layer-coated one at the charge voltage of 4.5 V. In a similar way, the Li-ion conductive solid-state electrolyte $Li_{1.5}Al_{0.5}Ge_{1.5}(PO_4)_3$ (LAGP) was demonstrated an effective coating material for LCO by Yang and coworkers [124]. The LAGP coating layer plays a role in stabilizing the LCO structure since the Ge ions can stabilize oxide ions on the surface of LCO by surface substitution as revealed by DFT simulation. Based on their functions, LAGP-coated LCO shows well-preserved crystal structures in both edge and inside of the cathode after cycling.

In the case of NCM cathode materials, Ni^{2+} cation can occupy the Li^+ site because the radius of Ni^{2+} cation (0.69 Å) is quite similar to that of Li^+ cation (0.76 Å). These phenomena induce subsequent structural changes, including phase transformation from layered to defect spinel and disordered rock-salt, greatly blocking the Li^+ ion migration [111,136,137]. Besides, these structural issues are severe at higher cut-off charge voltages with increased Li ion extraction. Uchida et al. [125] reported homogeneously coated NCM111 with ultra-thin Nb_2O_5 nanosheets. Raman spectroscopy indicates that Nb_2O_5 nanosheet-coated NCM111 preserves the layered phase after 100 cycles at 4.6 V charging while the bare NCM111 suffers from a noticeable growth of spi-

nel phase. This result verifies that the homogeneously deposited Nb_2O_5 nanosheets not only prevent the direct contact of electrode surface with electrolyte but also suppresses the phase transformation even at the high charging voltage. Kim et al. [126] constructed an intensified structure by nanostructured stabilizer on the surface of NCM811 cathode material. As shown in Fig. 5a, $Co(OH)_2$, as a stabilizer precursor, reacts with the residual Li compounds, such as LiOH and Li_2CO_3, and generates a nanostructured stabilizer during the sintering process. The resulting stabilizer is epitaxially changed from the spinel to the layered structure toward the core direction like a gradient. It is observed that the growth of the stabilizer precursor along the grain boundary creates a TM concentration gradient inside the cathode particle by scanning TEM (STEM). The nanostructured stabilizer and homogeneously distributed TM gradient stably maintain the TM composition in the cathode surface without Ni defects even after prolonged cycling, showing structural stability. The improved structural stability of gradient stabilizer coated NCM811 cathode is also observed by TEM with suppressed formation of cation mixing layer and Ni^{2+} ion dissolution after 500 cycles at 45 °C (Fig. 5b–d).

Additionally, inorganic phosphate compounds have been proven to be effective coating materials to overcome the structural stability issues of layered TM oxide cathode materials. Wang and coworkers [127] reported an ultrathin amorphous phosphate-coated NCA via a one-step H_3PO_4-ethanol corrosion process. As it has been reported that the diffusion of Li^+ from the NCA bulk to the surface could lead to the formation of surface residual Li species and induce an increase in Ni^{2+} concentration in NCA, correspondingly resulting in an increase in the Li^+/Ni^{2+} mixing and the polarization resistance [127,137]. The decreased cation mixing ratio in phosphate-coated NCA implies the effective maintenance of the bulk structure and the decrease of the surface residual Li species attributing to the trace doping of PO_4^{3-} ions into the NCA crystal lattice during the coating process. The zero shift of the (003) peak in the XRD patterns regarding the preserved length of the c-axis after 300 cycles further demonstrates the effect of the phosphate coating layer on the structure stabilization.

LMR cathodes face the challenge of structural degradation from monoclinic Li_2MnO_3. After the first charge, which involves the extraction of Li ions from Li_2MnO_3, the average discharge voltage decay could be observed during prolonged cycling because of consequent layered-to-spinel phase transition. As reported, such phase transition begins at the surface and grows toward the bulk during cycling [79,138,139]. Besides, the generated insulating rock-salt phases cause sluggish kinetics on the surface. To address these structural issues, various oxides [140–142] and fluorides [35,38,143–145] have been contributed as coating materials for LMR cathode materials. Ding et al. [35] reported NaF as a coating material that can establish a gradient $Na_{1-x}Li_xF$ layer on the surface of $Li_{1.2}Ni_{0.13}Co_{0.13}Mn_{0.54}O_2$ cathode. During the coating process, Na^+ ions were doped into Li^+ sites by Li^+/Na^+ exchange as presented in Fig. 5e. The structural stability of NaF modified $Li_{1.2}Ni_{0.13}Co_{0.13}Mn_{0.54}O_2$ is demonstrated by XRD patterns after cycling (Fig. 5f). The gradient Na^+ doping layer effectively suppresses the TM ions migration, resulting in the preserved layered structure. According to the coating advantages, the coated cathode shows 85% of capacity retention after 1000 cycles at 10C rate (Fig. 5g). Jiang et al. [146] reported that the spinel phase formed on the surface of $Li_{1.4}Mn_{0.6}Ni_{0.2}Co_{0.2}O_{2.4}$ (LMNC) cathode material through chemical Li-ion extraction during naphthalene sulfonic acid-doped polypyrrole (NPPy) coating can effectively enhance the structure stability of LMNC. During the first charge/discharge process, the NPPy coated LMNC shows not only a short plateau at ~4.5 V regarding electrochemical activation of Li_2MnO_3, but also a plateau at ~2.6 V, indicating the spinel phase. This newly formed spinel phase suppresses further phase transformation and operating voltage decay during 200 cycles by preserving their structure.

It should be noted that most of the surface coating strategies for structural stability accompany with doping or pillar to preserve crystal lattice during the high-temperature annealing, thus the cathode structural stabilization through surface coating in the above discussion may be more complicated.

Alleviating crack generation

Cracking in primary and/or secondary particles due to the anisotropic change of lattice parameters during cycling, especially at high voltages, long cycles and high temperatures, is an intrinsic problem for both LMO and LMR cathode materials. To make matters worse, the penetration of liquid electrolyte into cracks can accelerate side reactions on the grain boundaries, thus triggering severe capacity decay [136,137,147]. To address this terrible issue, many efforts have been focused [45,141–155]. Among the efforts, developing coating layers on the grain boundary by infusion is a feasible strategy to suppress the generation of cracks. Kim et al. [155] reported coating NCA with a glue nanofiller spinel-like Li_xCoO_2 layer. Coating on both inside and outside of the secondary particles is possible through the infiltration of ionized coating sources into the secondary particles via the gaps between each primary particle as exhibited in Fig. 6a. This well-developed glue-layer (G-layer) on the grain boundary was confirmed by HR-TEM images (Fig. 6b). Molecular dynamics (MD) simulations confirm the larger interfacial binding strength between the NCA host and the coating layer than that of the NCA/NCA interface, implying the key role of the G-layer in enhancing mechanical strength. Correspondingly, the G-layer-coated cathode delivers an outstanding cyclability with a capacity retention of ~87% after 300 cycles at both 25 and 60 °C (Fig. 6c). The G-layer-coated NCA cathode maintains the operating voltage during cycling at 60 °C, indicating a steady maintenance of the layered structure. Moreover, the G-layer-coated NCA cathode retains the pristine morphology of the secondary particle without any collapse after 300 cycles at 60 °C. Li_3PO_4 thin coating layer can also infuse into grain boundaries during the annealing process [37,156]. The studies of Li_3PO_4-coated $LiNi_{0.76}Mn_{0.14}Co_{0.10}O_2$ [37] and NCM811 [156] found that the grain boundary engineering effectively enables the protection of surface degradation and the suppression of intergranular cracking. This unique structure successfully prevents additional penetration of liquid electrolyte, leading to a stable interface which can contribute to the enhancement of structural and electrochemical properties. Following these advantages, Li_3PO_4-coated samples maintain a dense packing of the layered primary particles within the secondary particles after cycling.

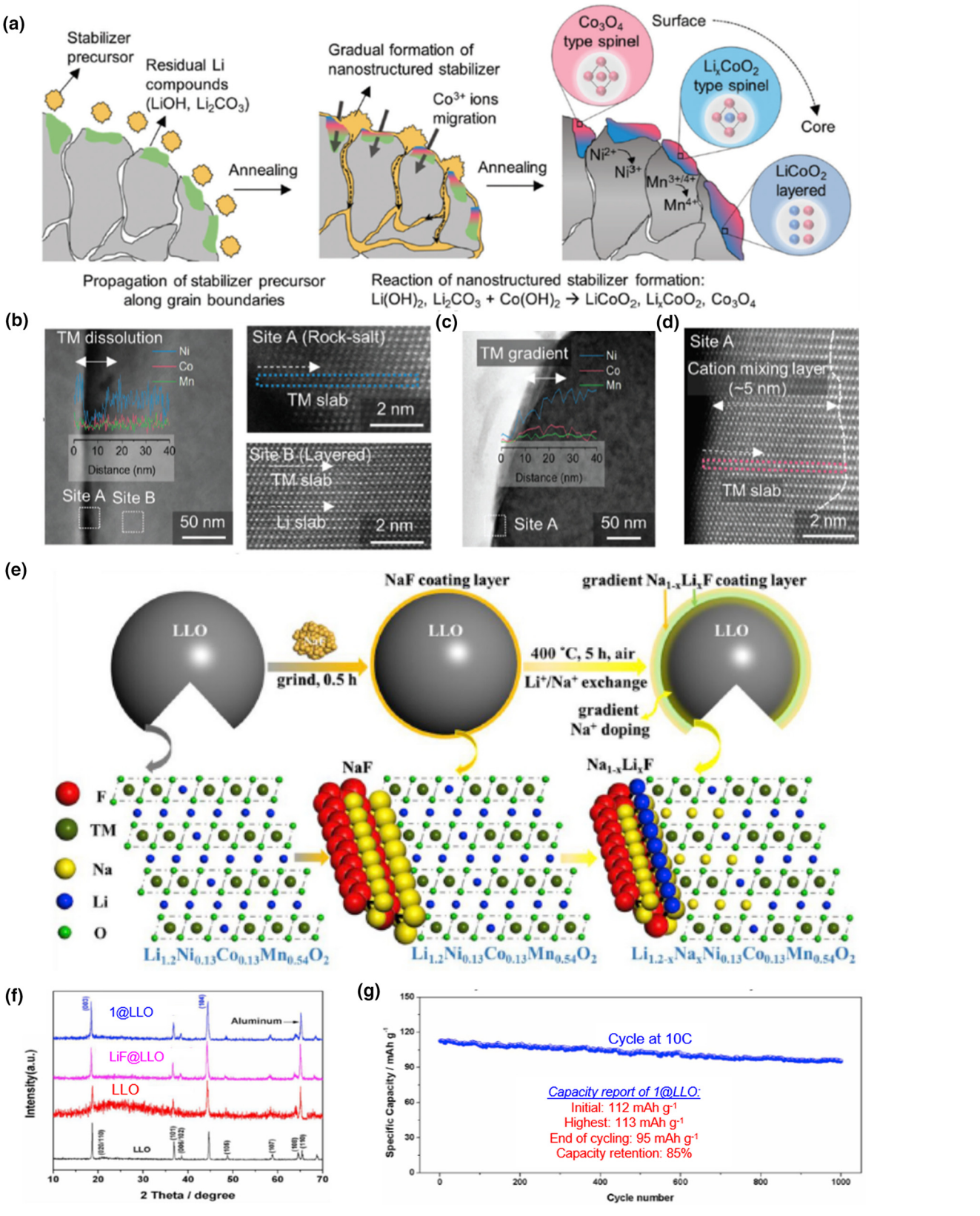

FIGURE 5

(a) Schematic of the synthetic process for the nanostructured stabilizer on NCM811 (NS-NCM), showing that the decomposition of the cobalt hydroxide compounds creates a nanostructured stabilizer with an epitaxial structure at the cathode and stabilizes surface TM oxidation states; (b) Magnified STEM images of the surface of the NCM, showing severe propagation of the cation mixing layer with a thickness of ~50 nm; (c) a magnified HAADF-STEM image of the NS-NCM with the line EDS result, indicating a robust surface compositional profile and (d) a magnified STEM image from site A. Reproduced with permission [126]. Copyright 2018, The Royal Society of Chemistry. (e) The schematic diagram of Li^+/Na^+ exchange process of $Li_{1.2}Ni_{0.13}Co_{0.13}Mn_{0.54}O_2$ cathode material. (f) The ex-situ XRD after 100 cycles; (g) the ultra-long cycling performance at 10C rate. Reproduced with permission [35]. Copyright 2019, Elsevier.

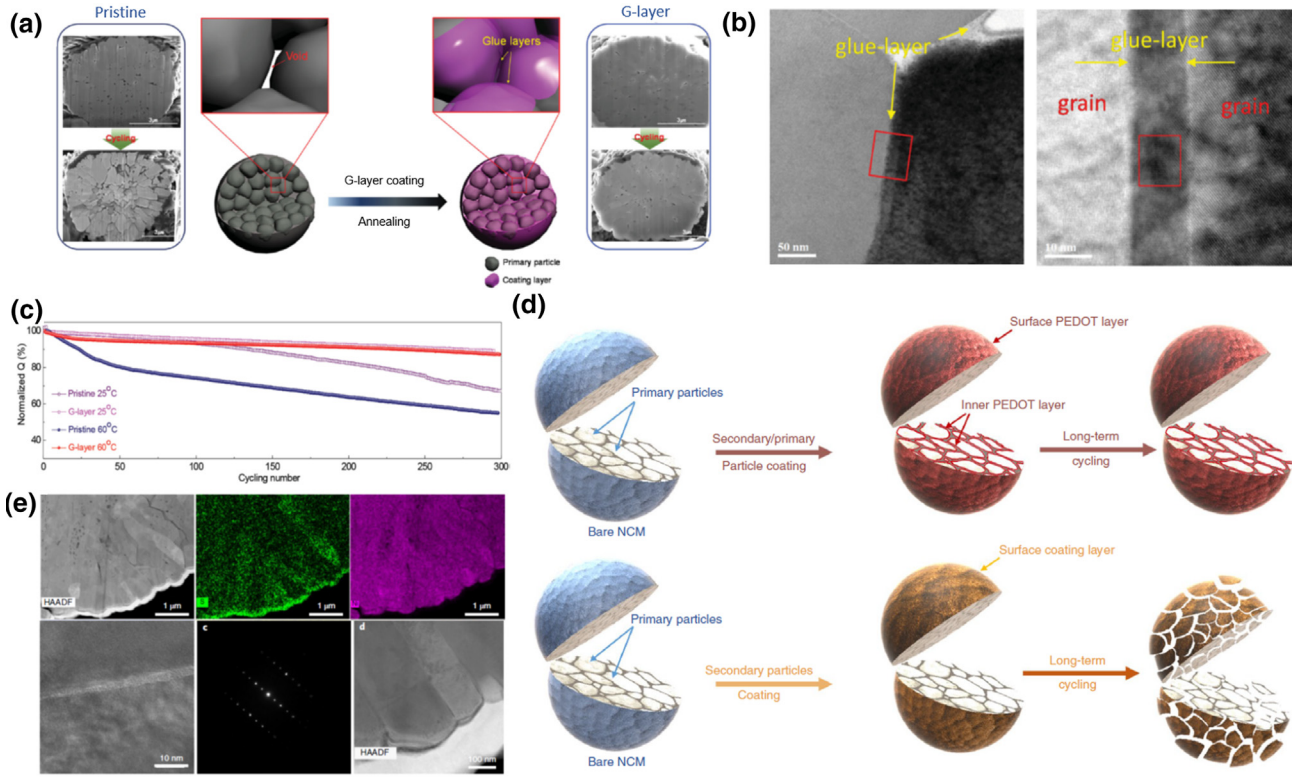

FIGURE 6

(a) The scheme of the formation of a glue layer (purple) among primary particles in a NCA secondary particle (gray) and the cross-sectional SEM images of the pristine G-layer coated NCA before and after cycling; (b) The HR-TEM images between grains of G-layer coated NCA, the right image is the expanded image of the red rectangle in the left image; (c) Cycling performance of the pristine and G-layer NCA samples between 3.0 and 4.3 V at 25 and 60 °C (charging rate: 0.5C; discharging rate: 1C). Reproduced with permission [155]. Copyright 2016, WILEY-VCH. (d) An illustration of the structural stability of both secondary/primary particle coating and only secondary particle coating after long-term cycling; (e) HAADF-STEM images and the corresponding EDS mappings of the PEDOT coated NCM111 cathode after 200 charge/discharge cycles at 1C in the range of 3.0–4.6 V. Reproduced with permission [45]. Copyright 2019, Springer Nature.

Very recently, Chen and coworkers [45] established a conformal, highly electronically conductive and ionically permeable PEDOT skin on the secondary and primary particles of NCM111, $LiNi_{0.85}Co_{0.1}Mn_{0.05}O_2$, and $Li_{1.2}Mn_{0.54}Ni_{0.13}Co_{0.13}O_2$ with an oxidative chemical vapor deposition (oCVD) technique (Fig. 6d). This electroconductive thin layer provides not only stabilized crystal structure but also a fast transport path of electrons and Li ions during cycling. According to their merits, PEDOT coated NCM111 cathode shows negligible intragranular cracking after 200 cycles in the voltage range of 3.0–4.6 V as presented in Fig. 6e. In addition, the PEDOT skin coated on secondary and primary particles of NCM111 brings improved thermal stability and structural stability due to the inhibition of the parasitic reactions between the delithiated layered cathode and the electrolyte. Moreover, the PEDOT skin is still well preserved without breaking or detaching after cycling as an evidence of its stable and sufficiently robust properties.

Enhancing oxygen redox

In the case of LMR cathodes, the irreversible release of lattice oxygen occurring with the extraction of Li ion during the first cycle at the surface inhibits the reversibility of the anionic redox ($O^{2-} \rightarrow O^{n-}$), which can also induce a large irreversible capacity loss and voltage decay [7,79]. $LiCeO_2$-coated $Li_{1.2}Mn_{0.54}Ni_{0.13}Co_{0.13}O_2$ was reported to be rich in O vacancies originating from the $LiCeO_2$ coating layer and such oxygen vacancies can effectively alleviate oxygen loss, stabilize lattice oxygen and enhance the reversibility of oxygen redox reactions, accordingly acting as a buffer for the migration of lattice oxygen in $Li_{1.2}Mn_{0.54}Ni_{0.13}Co_{0.13}O_2$ [157]. Moreover, $LiCeO_2$-coated cathode exhibits lower irreversibility of oxygen loss as indicated by cyclic voltammetry curves, thus contributing to the stable cycling performance. By avoiding irreversible oxidation of lattice oxygen, the charge-transfer resistance and TM-ion dissolution are also decreased. Li_2SnO_3 coating has been reported to be able to fabricate a small amount of spinel phase on the surface of LMR cathode because of the diffusion of Sn ions into the cathode material during lithiation [158]. This integration of coating layer and spinel phase enhances the reversible anionic redox activity and suppresses the lattice oxygen loss from the surface. It is demonstrated by X-ray absorption spectroscopy (XAS) and TEM that the Sn doping exists near the surface. Li_2SnO_3 coating layer with Sn doping and spinel phase provides a synergetic effect on the improved cell performance and structural stability with enhanced reversible oxygen redox reaction.

Strategies for increasing stability against moisture and air

Degradation by air and moisture during storage is a primary concern for Ni-based TM layered oxide cathodes, especially with Ni

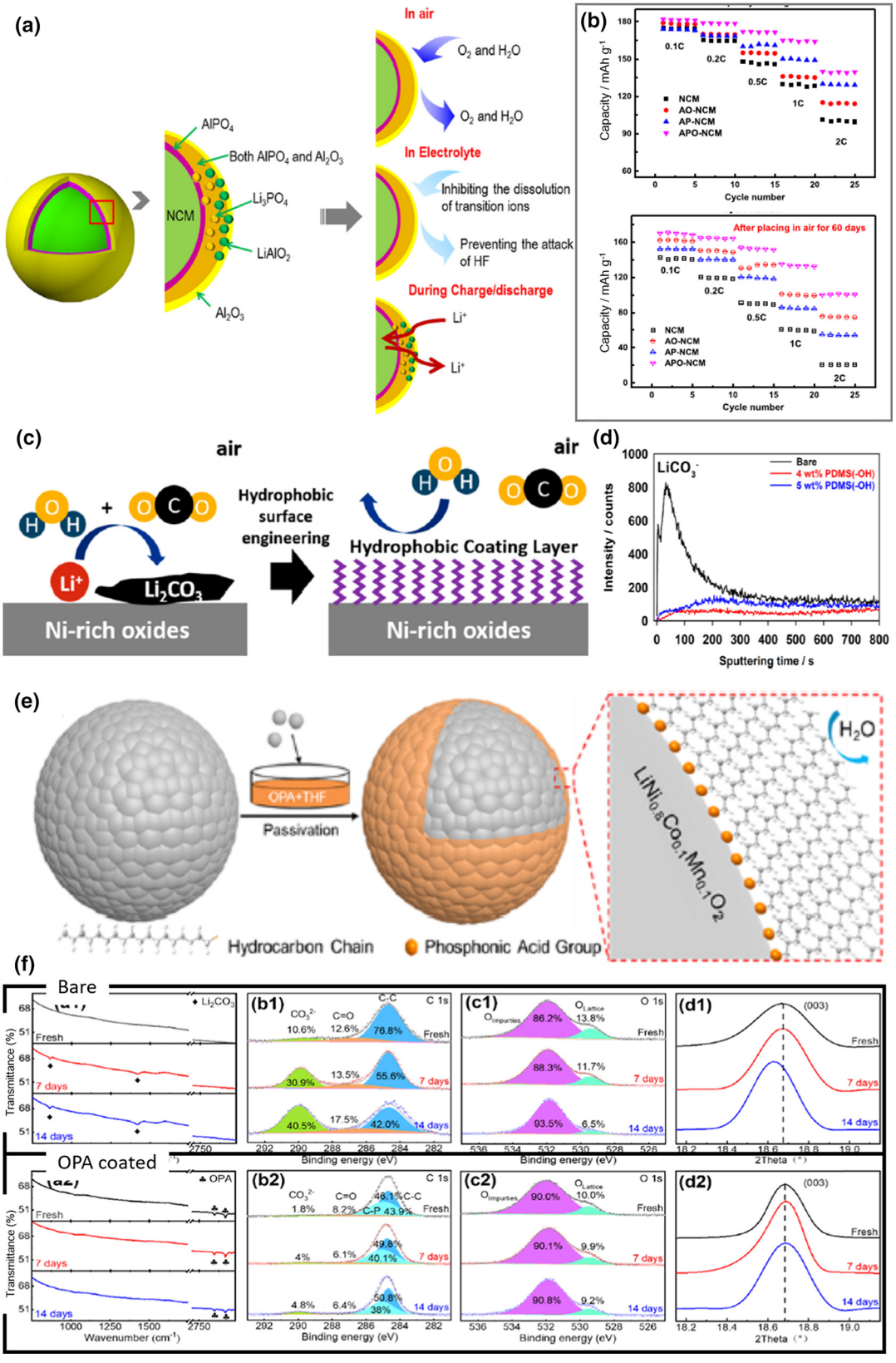

FIGURE 7

(a) Scheme of the possible working mechanism of the Al_2O_3–$AlPO_4$ double layers coated NCM523 during different circumstances; (b) Rate capability of the samples before and after placing in air for 60 days [160]. Copyright 2017, Elsevier. (c) Schematic concept of hydrophobic Ni-rich layered oxides; (d) TOF-SIMS depth profiles of $LiCO_3^-$ for bare, 4 wt.% PDMS(−OH)-grafted, and 5 wt.% PDMS(−OH)-grafted NCM811 powder samples after storing in a humidity chamber at 50% RH and 25 °C for 1 week. Reproduced with permission [163]. Copyright 2019, American Chemical Society. (e) Schematic illustration of the preparation process of SAM-passivated NCM811; f) FT-IR spectra, C 1s and O 1s XPS spectra, and the (003) peaks from the XRD patterns of bare and OPA coated NCM 811 at fresh and after being exposed for 7 and 14 days. Reproduced with permission [164]. Copyright 2020, American Chemical Society.

contents higher than 60% [159]. The reactions with H_2O and CO_2 from air on the cathode surface result in an accumulation of LiOH, which can react with $LiPF_6$ in the electrolyte, and Li_2CO_3, which decomposes and generates gas under high voltage as shown in the reactions from (8) to (11). In addition, such undesired chemicals formed through an exposure to air result in high resistance and polarization and low capacity for the cathodes. Therefore, the air-sensitive cathode materials need to be better protected for storage and transportation to avoid detrimental effects for practical batteries.

In general, any coating layers on the surface of cathode materials can act as shields to minimize the exposure to moisture, air, and other vaporized chemicals in environment. However, coating layers that effectively overcome the sensitive challenges without sacrificing the original electrochemical performances are more favorable. As one of the approaches to remove Li residues, some precursors of coating materials react with residual Li species on the cathode surface during the coating process as shown in reactions (18) and (19) [73,160].

$$6LiOH + Al(PO_3)_3 \rightarrow AlPO_4 + 2Li_3PO_4 + 3H_2O \quad (18)$$

$$3Li_2CO_3 + Al(PO_3)_3 \rightarrow AlPO_4 + 2Li_3PO_4 + 3CO_2 \uparrow \quad (19)$$

Several strategies, including coating with Li residue-reactive inorganic materials [96,161–163] and hydrophobic polymeric materials [164,165], are going to be introduced due to their effects on increasing the surface stability of cathodes against moisture and air. Zhao et al. [161] coated NCM523 with Al_2O_3–$AlPO_4$ double layers (Fig. 7a), which can prevent the attack of O_2 and H_2O in air as well as the HF in electrolyte. In addition, Al_2O_3 and $AlPO_4$ can react with Li_2CO_3 to generate some compounds such as $LiAlO_2$ and Li_3PO_4, which are beneficial for Li^+ transport from the bulk material to the electrolyte.

These coating effects contribute to benefits, including enhancement in cycling performance and thermal stability by mitigating the side reactions and superior rate capability after storing the cathode materials for 60 days in air, compared to the bare and the single layer coated NCM523 (Fig. 7b). Phosphate treatment to convert the undesirable Li residues on the surface of pristine high-Ni LMO to a protective Li_3PO_4 coating layer is also a simple but an effective approach to mitigate storage-induced degradation. Yang et al. [96] utilized phosphoric acid to form a Li_3PO_4 coating layer with extra carbon nanotubes (CNTs) penetrating, consequently constructing a multifunctional dense Li_3PO_4–CNT coating layer on the surface of NCM811. After exposing to air with high humidity for two weeks, the pristine NCM811 presents severe capacity decay during cycling while the Li_3PO_4–CNT coated NCM811 delivers quite similar capacity retention to the sample not exposed. Ryu et al. [162] reported a $(NH_4)_2HPO_4$ treatment on the surface of NCM811, which not only eliminates the Li residues on the cathode surface, thus inhibiting the formation of undesirable impurities, but also produces a thin Li_3PO_4 nanolayer protecting from H_2O and CO_2 infiltration during storage. After storing in a highly humid atmosphere (relative humidity: 70%) at 30 °C for 100 h, the pristine NCM811 shows severe cracking, which indicates the generation of residual Li compounds that reduce particle-to-particle adhesion among the primary particles by the penetration of moisture and air. In contrast, the Li_3PO_4-coated NCM811 effectively perseveres particle integrity from undesirable byproducts. These results prove that the dense and multifunctional coating layers greatly improve the stability of sensitive cathode materials against moisture and air. Recently, Xie and Manthiram have demonstrated that the treatment of an ultra-high-nickel cathode $LiNi_{0.94}Co_{0.06}O_2$ with phosphoric acid helps to maintain the morphology, rate capability, and cycle stability over 1000 cycles even after exposure to air for 450 days [163].

Constructing a hydrophobic surface on TM layered cathodes is another effective way to avoid the contact with moisture and air. Lee and coworkers [164] suggested that surface engineering using hydrophobic organic molecules, such as polydimethylsiloxane (PDMS) can result in a hydrophobic NCM811 cathode, as shown in Fig. 7c. The hydroxyl functional groups of PDMS can react with the hydroxyl groups on the NMC811 surface, forming TM–O–Si bonding during heating process. As shown in Fig. 7d, after storing in a humid chamber at 50% humidity and 25 °C for 1 week, a large amount of $LiCO_3^-$, one of the residual Li compounds, is observed on the surface of bare NCM811, indicating the serious reactions between the Li^+ on the surface of NCM811 and the H_2O and CO_2 in air. Whereas the PDMS-coated NCM811 shows a negligible amount of $LiCO_3^-$ because the hydrophobic surface inhibits the contact with moisture. Besides, the PDMS coated NCM811 enables negligible changes in the initial reversible capacity and cycle performance even after storage for 2 weeks. Gu et al. [165] reported using octadecyl phosphonic acid (OPA) based hydrophobic self-assembled monolayer (SAM) to coat the NCM811 cathode materials (Fig. 7e). OPA consists of hydrophobic long alkyl chain and phosphonic acid, which can interact with the surface hydroxyl groups on the cathode surface. The effects of the hydrophobic coating layer were investigated by Fourier Transform Infrared Spectroscopy (FT-IR) and XPS after ambient air exposure for 7 and 14 days (Fig. 7f). Compared with bare NCM811, the peak intensity of Li_xCO_3 species in XPS spectra significantly decreases in OPA-coated NCM 811. Furthermore, the OPA-coated NCM811 preserves structural stability with a negligible shift of the (003) peak after ambient-air exposure. While the (003) peak of the bare NCM811 is found to shift to lower angles, indicating a structural expansion along the *c* axis, which results from the extraction of Li ions by the formation of Li_2CO_3. This hydrophobic surface passivation strategy also delivers superior cell performance maintenance through stability against ambient air. The surface modification to mitigate the moisture and air sensitivity provides a robust interface which can control technical challenges during both electrode fabrication and cell operation.

Strategies for kinetics

According to the aforementioned instability issues, the increase in interfacial resistance by the formation of byproducts and structural collapse usually triggers the inhibition of Li ion and electron transport during cycling. A lot of efforts regarding increasing the kinetics have been made. However, some of the coating materials usually have only one function because they can barely cover both ion and electron conductivity simultaneously. For example, an excellent ionic coating may lead to a decrease in the electronic conductivity, and vice versa [166]. To

overcome these problems, coating strategies aiming to increase ionic conductivity have been developed and will be discussed in this subsection.

Improving ion transport

Solid-state Li ion conductors such as lithium boron oxide, lithium titanium oxide, lithium zirconium oxide, lithium silicon oxide, and metal phosphates as protective coating materials [30,43,167–186] have been demonstrated to be effective in overcoming these unavoidable challenges. As shown in Fig. 8a, Li_2ZrO_3 coating layer provides not only high ionic conductivity, but also gradient Zr^{4+} doping on the surface of NCM811 cathode material [43]. Li_2ZrO_3-coated NCM811 cathode exhibits a boosted capacity retention of 83.2% after 200 cycles because of the improved Li ion diffusion kinetics and both suppressed side reactions and structural degradation. In addition, a superior capacity of 164.7 mAh g^{-1} was obtained at 10C rate in a wide voltage window of 2.8–4.5 V (Fig. 8b). As reported by Liu et al. [168], $LiTiO_2$-coated NCA exhibits a high capacity retention of 90.8% after 100 cycles at 1C rate and a reversible capacity of 163.8 mAh g^{-1} at 10C rate in the voltage of 2.7–4.3 V. This improvement is attributed to the high Li ion diffusivity by the Li^+-conductive $LiTiO_2$ coating. In addition, the decrease in the residual Li compounds on the surface of Ni-rich cathode, consumed by the Li–Ti–O oxide coating process, should also be a contributor. $LiTaO_3$ has been selected as a coating material for enhancing the Li ion transport and stabilizing the surface structure of $Li_{1.2}Ni_{0.17}Mn_{0.56}Co_{0.07}O_2$ due to the piezoelectric property [30]. The diffusion coefficients of Li ion for $LiTaO_3$-coated samples exhibit negligible changes after cycling, resulting from the optimized Li^+ ion kinetics at the cathode surface, while the bare sample shows obviously a degraded value.

Li_3PO_4 is a popular coating material due to its high ionic conductivity ($\sim 10^{-6}$ S m^{-1}) as an Li-ion conductor. For this reason, Li_3PO_4-coated NCM811 cathode exhibits greatly improved Li ion diffusion and smaller charge-transfer resistance, resulting in superior interfacial kinetics [177]. In addition, Li_3PO_4-coated NCM811 cathode is demonstrated to have decreased amount of residual Li species (which are detrimental to Li ion transport) on the surface of the cathode particles. $MnPO_4$ is also suggested as a favorable coating material for its natural abundance and environmental benignity as well as its high structural and thermal stability, as well as the ability to enhance charge transfer at the cathode/electrolyte interface [178,179]. Accordingly, $MnPO_4$ coating layer leads to a substantially enhanced cycling stability of the $LiNi_{0.4}Co_{0.2}Mn_{0.4}O_2$ (NCM424) cathode even under a high-rate condition of 10C during 100 cycles [178]. Moreover, the full cells of $MnPO_4$-coated NCM424 cathode and graphite anode provide a capacity retention of 74.1% after 2000 cycles at 1C rate, allowing for energy and power densities of 376 Wh kg^{-1} and 1841 W kg^{-1}, respectively, on the active material level. NASICON-type solid electrolyte $LiZr_2(PO_4)_3$ (LZP) has also been applied on the surface of NCA cathode to enhance the Li^+ diffusion in the interface of electrode/electrolyte and to prevent the side reactions of cathode with electrolyte [182]. This advantage is demonstrated by that LZP-coated NCA shows a higher Li^+ diffusion coefficient than pristine NCA even after 300 cycles. Additionally, the electrode polarization and voltage degradation of NCA cathodes are also effectively alleviated because of the LZP coating. $Li_3V_2(PO_4)_3$ (LVP) is chemically stable and electrochemically active in terms of partial oxidation of V^{4+} to V^{5+} at 4.6 V [186]. Therefore, employing it as a coating material, LVP will not only be a good Li ion conductor in cathode materials but also can deliver additional reversible capacity. These are well demonstrated with LVP-coated $Li_{1.17}Ni_{0.2}Co_{0.05}Mn_{0.58}O_2$ cathode, which obtains sustainable cycling performance with higher reversible capacity and better thermal stability than the uncoated one.

As one of the strategies for improving interfacial ion transport, spinel-type electrode active materials that have a 3D transport channel have been investigated as coating materials [187–191]. $Li_4Ti_5O_{12}$ (LTO), as a well-known anode material, has a Li^+ transference number of 0.99 and a high Li^+ diffusivity of 1×10^{-6} cm^2 s^{-1} (at ~900 °C) [192]. Zhou et al. [189] reported LTO-coated LCO cathode material by a sputtering process. The LTO-coated LCO delivers a reversible capacity of 113 mAh g^{-1} at 12C rate, which is 70% higher than that of the uncoated cathode due to the high intrinsic Li^+ diffusivity of LTO. Spinel-type $LiNi_{0.5}Mn_{1.5}O_4$ (LNMO) coating has been reported not only to prevent side reactions with electrolytes but also most importantly to greatly facilitate Li ion transport in the $0.4Li_2MnO_3 \cdot 0.6LiNi_{1/3}Co_{1/3}Mn_{1/3}O_2$ cathode as revealed by the improved structural/electrochemical behaviors [187]. Subsequently, the intrinsic 3D Li^+ diffusing channels of LNMO enable the coated sample to deliver a capacity of 170.7 mAh g^{-1} with a capacity retention of 94.4% after 100 cycles at 5C rate [187]. Very recently, Han et al. [193] reported poly(methyl methacrylate) (PMMA) nanolayer coated single-crystal (SC) NCM811 cathode. The ester group in PMMA, as an electron-absorbing group, is able to interact with the interfacial Ni^{2+}, resulting in the formation of a nickel–polymer robust interface. The PMMA coating layer on SC NCM811 allows improved Li ion diffusion and inhibits the dissolution of Ni cation from the high specific surface area. The PMMA coated SC NCM811 shows a discharge capacity of 157.8 mAh g^{-1} even at a 20C rate.

Improving electronic conductivity

In this subsection, for the ability of improving electronic conductivity, electronic conductive materials, such as carbon-based compounds and conducting polymers, will be introduced. Moreover, surface modification using materials combining electronic and ionic conductivities will simultaneously be presented as a multifunctional coating strategy.

Electronic conductive materials which provide electron transport networks on the surface of the cathode when acting as a coating layer, can help reduce the interfacial resistance [44,84,85,194–201]. rGO sheets are considered as preferred coating candidates due to their highly conductive property and their ability to completely wrap the surface of cathode materials, as reported in several studies [84,85,196,197]. The electrical conductivity of rGO-encapsulated NCM622 surface is confirmed with atomic force microscopy (AFM) technique through current image with increasing applied voltage [196]. This highly electronic conductive sheet provides not only improved electrochemical performance but also better thermal stability resulting from reduced interfacial side reactions with the electrolyte under coating. Very recently, Chen and coworkers reported aluminum-

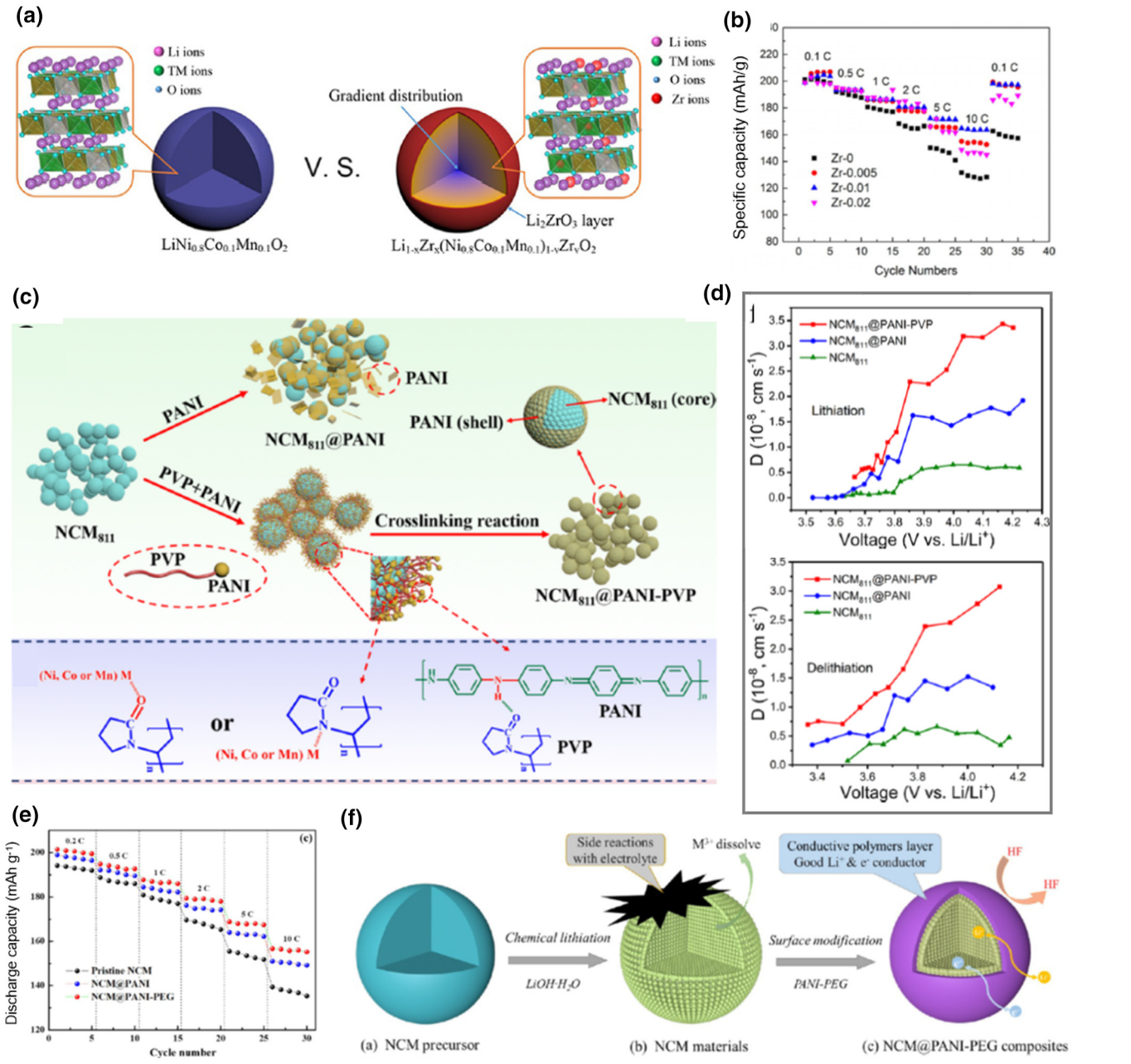

FIGURE 8

(a) Schematic diagram of Li_2ZrO_3 coated NCM811 cathode; (b) C-rate properties for bare and Li_2ZrO_3 coated NCM811 cathodes at 2.8–4.5 V. Reproduced with permission [43]. Copyright 2018, Wiley-VCH. (c) Schematic illustration of the preparation of PANI-PVP coated NCM811 and possible reactions among NCM811, PVP, and PANI; (d) Diffusion coefficients calculated from galvanostatic intermittent titration technique (GITT) potential profiles as a function of potential during lithiation and delithiation. Reproduced with permission [44]. Copyright 2019, American Chemical Society. (e) Rate performance of PANI-PEG coated NCM811, PANI coated NCM811, and bare NCM811 cathodes; f) Schematic illustration of the synthesis and coating effects of PANI-PEG coated NCM811. Reproduced with permission [195]. Copyright 2018, American Chemical Society.

doped zinc oxide (AZO)-coated LCO cathode [202]. AZO is a well-known conducting oxide with suitable electronic conductivity to stand a chance of improving C-rate capability. The uniform AZO coating layer generated by wet-mixing delivers higher electronic conductivity for AZO-coated LCO (3.92×10^{-4} S cm^{-1}) than for bare LCO (7.32×10^{-5} S cm^{-1}). The enhanced rate capability is proven to be due to an advantage of this coating layer. Further AZO-coated cathode achieves long-term cycling stability based on surface protection and superior kinetics of the AZO coating layer.

Compared to carbon-based materials, electron conducting polymers such as PPy, PANI, and PEDOT could be preferable coating layers on the surface of cathode materials because of their high electronic conductivity and electrochemical/thermal stability [44,45,194,195,203]. Their metallic conductivity is usually obtained by doping, in which the dopant can not only with-

draw electrons from the conducting polymers but also add electrons to the backbones of the conducting polymers [204] Lu and coworkers [44] reported a uniformly anchored NCM811 cathode by the bonding effect between the pyrrolidone rings of PVP and –NH– groups of PANI as presented in Fig. 8c. Due to the bonding effect, the electroconductive PANI layer can be uniformly anchored onto the cathode surface with the help of PVP when compared with the randomly distributed PANI-only coating. This stable PANI-PVP coating layer not only serves as the rapid channel for electron conduction but also relieves the volume expansion of the NCM811 cathode material to deliver higher rate capability and better capacity retention upon cycling than the pristine and the PANI-only-coated samples. In addition, the coating layer stably preserves upon the repeated charging-discharging process. *In-situ* XRD and *in-situ* Raman results during the extraction/insertion of Li ions further confirm the crystalline structure stability of the PANI-PVP-coated cathode. In addition, PANI-PVP-coated NCM811 cathode exhibits much higher diffusion coefficients, demonstrating that the PANI-PVP coating layer can facilitate the diffusion of Li ions (Fig. 8d).

Besides the coating layer formed by sole electronic conductive polymers, the combination of electronic conductive polymers and ionic conductive materials has also been reported as coating layers to improve the charge transfer on the surface of layered TM oxide cathodes, though the electronic conduction of the combination layers is reduced compared to that of the coating layers with sole conductive polymers. For instance, Cao et al. introduced the poly(ethylene glycol) (PEG) as an ionic conductive polymer into the PANI coating layer [195]. The electronic conductivity of PANI-PEG-coated NCM 811 cathode is tested to be 2.85×10^{-2} S cm^{-1}, much higher than that of bare NCM811 cathode (1.74×10^{-5} S cm^{-1}). It can be clearly observed that the rate capability of the PANI-PEG-coated NCM811 (156.7 mAh g^{-1} at 10C rate) is better than that of the bare NCM811 (139.4 mAh g^{-1} at 10C rate) in the voltage range of 2.8–4.3 V (Fig. 8e). Besides, the PANI-PEG coating layer suppresses TM dissolution, resulting in an enhancement in the cycling performance at 55 °C. The PANI-PEG-coated NCM811 cathode also exhibits the lowest amounts of dissolved TM after the same storage time because PEG can complex with PF_5, consequently preventing the hydrolysis of PF_5 to generate HF that triggers TM dissolution (Fig. 8f). In a similar way, Li_3PO_4 as a high ionic conductor is combined with electronic conductive PPy for a coating layer on NCM811 cathode [46]. According to the synergetic effects, the PPy-Li_3PO_4 coating layer not only prevents side reaction through HF scavenging but also brings superior rate performance due to the high electronic conductivity. Moreover, PPy-Li_3PO_4-coated NCM811 cathode materials greatly suppress the crack generation during cycling while maintaining the coating layers during cycling.

The above results suggest that most of the approaches with electronic conductive polymers have shown highly improved electrochemical performances. However, it should be indicated that for achieving a stable surface at high voltage, the electrochemical stability of electron conducting polymers should also be considered because they commonly have a narrow gap between the lowest unoccupied molecular orbital (LUMO) and the highest occupied molecular orbital (HOMO).

Surface modification methods

Currently, the often-used surface modification methods include: (1) conventional chemical coating methods, such as co-precipitation, sol–gel, hydrothermal, and solid-state; (2) physical techniques such as spray dry method, pulsed laser deposition (PLD), physical vapor deposition (PVD) and CVD; and (3) advanced deposition methods, such as atomic layer deposition (ALD) and some modified ALD like ASR and molecular layer deposition (MLD). The starting bulk materials for surface modifications are mostly the pristine cathode powders, while the ones for concentration gradient structures mainly begin with the raw chemical sources of the cathodes, and a few are synthesized based on the precursors of the cathode materials. The basic experimental steps of the main methods are depicted in Fig. 9.

Conventional chemical coating methods

Co-precipitation, sol–gel, hydrothermal, and solid-state methods have been widely used in cathode materials to achieve surface coatings. In these methods, the raw coating materials are normally not the finial chemical composition of the coating layer. A calcination step is essential at the end of the coating procedure for all these methods (in some cases, this is not needed as in a hydrothermal coating method) to finalize the coating layer with the expected chemical formula. The differences lie in the mixing way and the status of the raw coating materials. Among them, solid-state method is the easiest way to realize coating because it just needs to mix the coating materials with cathode precursor and Li source or cathode powder and then to conduct calcination, but it is hard to control the thickness and uniformity of the coating layer. Sol-gel coating method is to mix the raw coating material with cathode precursor or cathode powder in a sol state, which will be in favor of the uniform distribution of the coating material due to the low fluidity of the sol solution and the following gel state. After calcination, whose heating temperature is usually lower than that in a solid-state method, a relatively uniform coating layer can be formed on the surface of cathode particles. However, the thickness of the coating layer is still hard to be controlled precisely. Hydrothermal coating method is based on the operating mechanism of hydrothermal reaction, in which the raw coating materials are mixed with the raw materials or the precursors of cathodes and undergo chemical reactions in solution state under low temperatures (mostly lower than 200 °C) to achieve cathode materials with coating layers. Compared to other coating methods, hydrothermal coating method is more economic due to the low operating temperature and less procedures, but it is limited by the specialized reactor and the high pressure reaction environment, making it difficult to be applied in large scale production. The major coating materials of layered TM oxides used in these conventional chemical coating methods are metal oxides, phosphates, fluorides, solid-state electrolytes (ion conductors), polymers, and carbon materials (electron conductors). AlF_3 and $LiAlF_4$ have been reported to coat on $Li_{1.2}Ni_{0.2}Mn_{0.6}O_2$ by post-calcination treatment [205]. $La_{0.8}Sr_{0.2}MnO_{3-y}$ has been introduced as a protective and phase-compatible surface layer on $Li_{1.2}Ni_{0.13}Co_{0.13}Mn_{0.54}O_2$ cathode by a solid-state method [206]. F-doped Li_2SnO_3 [207] and Zr-containing phosphate [208] coated Li[$Li_{0.2}Ni_{0.17}Co_{0.07}$-

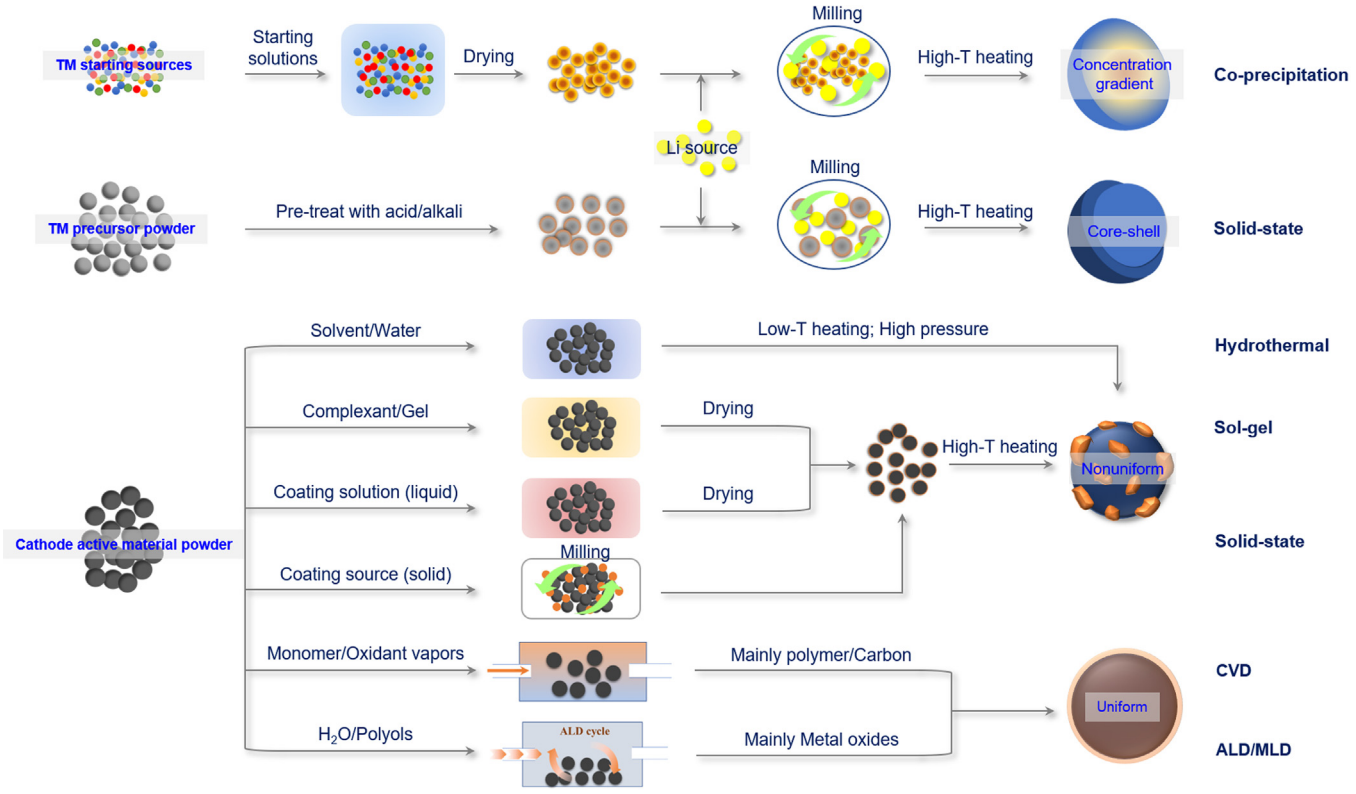

FIGURE 9

Schematic diagram summarization of surface modification techniques. In general, High-temperature (High-T), Moderate-T and Low-T heating indicate the operating temperature higher than 400 °C, around 200–400 °C and lower than 200 °C, respectively.

$Mn_{0.56}]O_2$ can be obtained by a sol–gel method. Recently, Ding et al. designed a three-in-one surface treatment via a solvent hydrothermal reaction to enable oxygen vacancies, spinel phase integration, and N-doped carbon nanolayer synchronously built on the surface of $Li_{1.2}Mn_{0.6}Ni_{0.2}O_2$ microspheres [55].

Co-precipitation coating method is based on a co-precipitation reaction, followed by high temperature calcination. It is the dominating synthesis method for core–shell compounds, including hierarchical architectures and CG structures, which have been demonstrated as a significant breakthrough in high energy LIBs with superior cyclability and thermal stability [56,209,210]. Kim et al. have developed a differential co-precipitation process to synthesize a multi-compositional particulate $LiNi_{0.9}Co_{0.05}Mn_{0.05}O_2$ cathode in which $LiNi_{0.94}Co_{0.038}Mn_{0.022}O_2$ at the particle center is encapsulated by a 1.5 μm thick CG shell with the outermost surface composition $LiNi_{0.841}Co_{0.077}Mn_{0.082}O_2$ [211]. Sun et al. utilized the co-precipitation method to realize nano-functional full-gradient $LiNi_{0.75}Co_{0.10}Mn_{0.15}O_2$ with the Ni concentration decreasing linearly, whereas the Mn concentration increasing linearly from the center to the outer layer of each particle [58]. Besides co-precipitation, core–shell compounds also have been synthesized through pre-treating the precursor of cathode materials with $NH_3{\cdot}H_2O$ and followed by a solid-phase reaction process [212]. Although co-precipitation method to realize the core–shell materials can achieve dense and highly conformal surface layer, and the compositions of the core and the shell as well as the ratio of the core to shell can be precisely controlled, it requires more complicated processing procedures, and the enhancement of cathode performance is subject to the composition of the coating material.

These conventional techniques mostly offer important advantages of easy operation, less limitation on coating materials, and low cost, enabling the suitability for commercialization. However, they still face critical technical challenges to precisely control the thickness of the coating layer and to ensure a homogeneous distribution of the coating layer on the surface of cathode particles, since the uncoated sections will be exposed to the electrolyte, causing undesirable performance decay of LIBs. In addition, the high-temperature calcination (>600 °C) inevitably leads to a deterioration of the bulk structure of the materials.

Conventional physical coating methods

Conventional physical coating methods include *in-situ* formed coating technologies, such as spray drying [213], and deposition methods, mainly PLD, PVD and CVD [65,214]. Spray drying for coating has a simple preparation process, in which the coating material and cathode powder are mixed in solutions and then rapidly dried with a hot gas. It is a suitable technology applicable for large-scale production with various coating materials, but the thickness and the uniformity of the coating layer is difficult to control. PLD is typically a PVD technique and often used to deposit coating layers on cathode electrode. In a PLD coating, a high-power pulsed laser beam is focused inside a vacuum chamber to strike the coating material, then it is vaporized from the target (in a plasma plume) and deposits as a thin film on the sub-

strate (i.e., the cathode). However, the PLD coating method suffers from poor interface compatibility between the active material substrate and the surface layer, which will lead to a detachment of the coating layer from the bulk material during repeated cycling.

CVD employs a single step to convert the vapor phase monomers to solid polymeric thin films. Generally, a CVD process consists of the exposure of the substrate (i.e., cathode material here) to one or more volatile compounds (i.e., the coating materials here), the gasification of the coating material and subsequently the chemical reaction or decomposition on the substrate surface to produce the desired thin film deposits. It is uniquely poised for growing layers of insoluble macromolecules and the deposited layer could be monocrystalline, polycrystalline, amorphous, and epitaxial. oCVD technique is developed based on CVD. In analogy to CVD methods for inorganic thin films, varying the conditions of the oCVD process permits a systematic tuning of film characteristics, including electrical conductivity, optical transparency, work function, and crystallite orientation. Chen et al. reported an oCVD technique to build an ultra-conformal, protective and electronically conductive PEDOT skin at both secondary and primary particle levels of both NCM and LMR [45]. Through CVD and oCVD, a more compact and uniform surface layer can be established, and the thickness can be tuned and precisely controlled, but it is hard for them to be commercialized due to the high dependence on expensive apparatus.

ALD and ALD-based deposition methods

ALD is a unique vapor-phase technique capable of producing thin films of a variety of materials and has been widely used in surface modification of cathode materials. A general ALD coating process is based on sequential and self-limiting reactions, in which the coating material is pulsed into a chamber under vacuum to fully react with the cathode material surface through a self-limiting process, followed by the counter-reactant coating material pulse and purge, creating up to one layer of the desired coating material. This process is then cycled until the appropriate film thickness is achieved. With the assistance of ALD, metal oxides such Al_2O_3, TiO_2 and ZrO_2 [211,215–217] and solid-state electrolytes with high ionic conductivity and thermal stability, such as $LiAlF_4$ [218] and $LiTaO_3$ [219] can be homogeneously deposited on the surface of LMO and LMR cathode materials. Moreover, Zhang et al. combined ALD followed by a calcination process at 600 °C to enable a uniform Li_3PO_4 layer coated on the secondary particles of $LiNi_{0.76}Mn_{0.14}Co_{0.10}O_2$ and the infusion of Li_3PO_4 along the grain boundaries of the primary particles, thus achieving fast channels for Li-ion transport and simultaneously preventing penetration of the liquid electrolyte into the boundaries [37]. This coating approach provides designing ideas for advanced cathodes. In ALD method, the thickness of the deposited layer can be controlled by adjusting the ALD cycles, correspondingly an atomic-scale ultrathin coating with excellent uniformity, flexibility, and conformity can be easily obtained. However, one of the major drawbacks of the ALD method is its high cost and extremely low efficiency, which is difficult for mass production.

ASR is a surface modification method developed based on ALD. It is a simple, facile, and non-conventional vapor phase chemical treatment with a reactive species that will selectively reduce the interface of the functional material, without changing the bulk structure [110]. Noked and coworkers reported that utilizing the vapor phase of reactive organometallic compounds (*e.g.*, TMA) at relatively low temperatures, ASR can alter the electronic structure of surface Mn and Ni in $0.35Li_2MnO_3 \cdot 0.65LiNi_{0.35}Mn_{0.45}Co_{0.20}O_2$, leading to higher stability and reduced parasitic reactions [61]. Compared to ALD, extremely conformal coating with controllable thickness can also be obtained by ASR, but with less time-consumption and no alternating precursor sequence. However, since sharing the similar operating mechanism with ALD, ASR is still subjected to a vacuum reacting environment and vapor phase chemical treatment, which makes the ASR coating process harder and costlier than the aforementioned conventional coating methods.

MLD is another technique analogous to ALD, in which organic–inorganic hybrid films and all-organic coating can both be deposited. The coating process of MLD is in a similar fashion to ALD, in which the coating materials are pulsed on a sequential, cyclical manner, and all gas–solid reactions are self-limiting on the cathode substrate. In an ideal case, the repeated MLD cycle could build up an organic/inorganic monoatomic layer at a time, enabling highly conformal coatings with precise thickness control and purity. Similar to ALD, the operating cost is relatively high and it has rather strict chemical limitations for coating materials to be suitable for this coating method. Recently, Kong et al. reported a uniform C-Al_2O_3 composite coating with homogeneous thickness on NCM622 by the pyrolysis of molecular layer deposited alucone in argon [220]. In the MLD coating process, the pyrolysis of hybrid film could easily form a nanoporous oxide layer with large specific surface area and simultaneously the pyrolysis of alucone in inert atmosphere can lead to a conformal C-Al_2O_3 composite coating layer [221], which has a much lower sheet resistance than the pure Al_2O_3 film [222]. Up to now, the reports of hybrid organic–inorganic or all-organic coating on TM layered oxides cathodes are still extremely limited.

Definitely, ALD and the ALD-derived coating methods offer exceptional advantages of excellent uniformity and conformity, thickness control at atomic-scale, and tunable film composition, as well as low growth temperatures, which are difficult to realize simultaneously by other coating techniques. However, when it comes to large-scale deposition in practical applications, designing economically feasible and easy-to-operate reactors for ALD methods are required. It is also a critical challenge to obtain a multipurpose coating that comes with two or more functionalities to solve the surface stability issues in one modification process.

Summary

The abovementioned surface modification methods can be divided into different categories depending on the specific properties required. The conformity and thickness of the coating layer are key factors for the performance of coated materials. If a uniform coverage is needed, CVD, ALD and MLD are absolutely recommended because they allow the fabrication of uniform layers on the surface of cathode materials with controllable thicknesses. The limitations of these techniques are high cost and time-

consuming process, which greatly inhibit their applications on a large scale. On the other hand, sol–gel, hydrothermal and solid-state methods can provide easier processes and lower costs than the aforementioned ones. However, it is hard for them to achieve controllable uniformity and thickness as shown in Fig. 9. Hence, further efforts are required to find out advanced surface modification technologies to cover all the conditions.

Perspective

The instability of layered TM oxides cathode materials can lead to an early failure of LIBs. Surface modifications have been well-established as effective strategies to improve their physical, chemical, and electrochemical stabilities. An ideal protocol of surface modification should meet the requirements that improve the stability and electrochemical behavior of cathode materials without sacrificing the performances. It should be pointed out that the thickness and dense condition of the coating layers have great impacts on the battery performance of the coated materials. If the coating layer is too thin, the protection on the cathode materials is not robust enough to promise good battery performance during prolonged cycling as expected. However, if the coating layer is too thick, the increased resistance of the coating layer will lead to high polarization during the charge/discharge processes, thus lowering the cell capacities (although the cycling stability of the cathode materials may be achieved). On the other hand, the impact of the density or dense condition of the coating layer on the battery performance has seldom been reported. It is reasonable to speculate that if the coating layer is of a porous structure, the protection of this layer to the cathode materials would not be effective. Then, the battery performance of the cathode materials could be improved a bit but not much. Therefore, for a conventional surface coating, a uniform and dense coating layer with an optimized thickness and continuous distribution will be always favorable for maximally protecting the cathode materials without impeding electronic or ionic conductivity. Additionally, when choosing coating species, it is necessary to take the bonding strength between the resulting coating layer and the surface of the cathode into consideration. Inferior bonding of the coating layer to the cathode surface will result in particle collapse by the high-pressure during the electrode calendaring process and/or boundary discontinuity contributed by the lattice volume changes during long-term cycling, both of which will lead to drastic decline in the battery performance [223,224]. When it comes to industrial application, the cost of the coating materials should also be taken into consideration as the consumption will no longer be underestimated. For example, the polymer coating materials, such as PMMA and PVP, have a relatively affordable price of ~$300 per kilogram while conducting polymers like PEDOT and PANI have a much higher price of ~$10,000 per kilogram according to chemical vendors when selling at small quantities. Inorganic materials have also a range of prices in the market depending on their precursors and synthesis methods. Therefore, the cost of coating materials should be an additional criterion when choosing coating species for surface modification in industrial production.

Undoubtedly, a variety of surface modification strategies have been demonstrated to considerably address the instability issues of cathode materials. Modification strategies, such as surface coating and core–shell structure, are effective in addressing part of surface problems, including phase transformation, TM ion dissolution, electrolyte decomposition, and particle cracking, but are insufficient to cover all destructive challenges to enable satisfactory electrochemical performance for commercialization. Moreover, favorable effects in the reported surface strategies are always accompanied with some undesirable consequences. For instance, inert surface coating is an effective remedy for undesirable interfacial reactions but always accompanied by the impediment of charge transfer on the cathode surface [17]; core–shell structure can enable superior thermal stability, but prone to boundary cracks between the core and the shell after cycling because of the different degrees of the lattice volume changes [224]. Therefore, combining different surface treatment methods in one modification protocol is expected to involve individual merits of each method to exhibit cooperative or synergistic effects on addressing multiple stability issues on the surface of cathodes.

Although many coating materials are multifunctional, they cannot be expected to have a universal coating effect for all the layered TM oxide cathodes because each of them has its specific problems as mentioned in the above section. Recently, several reports have mentioned the chemical cross talk between anode with cathode that could be a universal problem for all batteries [225–227]. Some species such as fluorinated compounds including HF, CH_xF_y, and $POF_x(OH)_y$ as well as carboxyl (>C = O) compounds can dissolve in electrolytes, then move across the separator and react with or deposit on the cathode surface, resulting in thick and resistive CEI layers. In addition, dissolved TM cations from the cathode cause high overpotentials and also lead to a non-uniform distribution of Li deposits. In this regard, although there are now no reports about the effect of cross talk of reduced species from Li anode on the coating materials on the cathodes, the side reactions between the coating materials and the cross talk species should be considered when using the cathode coating materials in the future. Meanwhile, as one of the efforts to achieve high energy density battery, cathode materials with high operating voltages have garnered as a candidate for next generation batteries [10,228]. The coating materials, which have inferior electrochemical oxidation stability than the operating cathode, may cause unexpected irreversible reactions, leading to diminishing cell performance. Thus, the oxidation stability of coating materials should be considered as well; otherwise additional issues will arise.

The hybrid modification strategies would be promising for further development of cathodes applied in commercial LIBs. However, the following aspects should be considered when a proper hybrid modification strategy is designed. First, it is not a process by simply mixing several surface treatment methods. Second, more efforts of surface modifications should be devoted to remedying the unexpected instabilities induced by more aggressive surface chemistry with the increase in Ni content in LMO and by new redox chemistry, oxygen redox reaction, involved in LMR systems. This is urgently needed because Ni-rich LMO and LMR are two series of cathode materials that have attracted worldwide attention as potential next-generation cathodes for EV batteries [147,229–231]. Third, single crystalline particles

are greatly beneficial to the volumetric energy density and simultaneously possess higher mechanical strength than polycrystalline cathode particles [231]. While few studies have been reported on the surface modification of single crystalline layered oxides cathodes, such work is urgently needed. Fourth, it is currently limited to verify the feasibility of the surface engineering for the commercialization under the industrial manufacturing conditions. The effects of most surface modifications are verified under low electrode density and cathode loading. However, the scale-up feasibility of surface treatment process and the electrode pressing process, which involves high-pressure calendaring, are largely ignored in most reports. These may give rise to large deviations when applying the surface modification strategies or surface modified cathodes in industrial manufacturing. Hence, the future direction in surface modification studies should include the evaluation of various surface modification strategies under practical conditions. An optimized surface modification in industrial manufacturing should achieve a balance among coating material cost, processing cost (including time consumption, operational complexity and machining precision or effective conversion rate) and the ultimate effects on enhancing the specifically required performance of cathode materials in practical applications. Overall, surface engineering is all about getting layered TM oxides consistently to give the best performances, motivating them to grow to their fullest potential and enabling them to apply in EV markets.

Author contributions

W.X. initiated and supervised the writing of this review paper. J.-M.K., X.Z. and W.X. wrote the paper. J.-G.Z., A.M. and Y.S. M. gave critical and constructive comments and revised the paper.

Declaration of Competing Interest

The authors declare that they have no known competing financial interests or personal relationships that could have appeared to influence the work reported in this paper.

Acknowledgements

This work was supported by the Assistant Secretary for Energy Efficiency and Renewable Energy, Vehicle Technologies Office of the U.S. Department of Energy (DOE) through the Advanced Battery Materials Research (BMR) program (Battery500 Consortium) under the contract no. DE-AC05-76RL01830.

References

[1] I. E. Agency, Global EV Outlook 2019, https://www.iea.org/reports/global-ev-outlook-2019, (accessed May, 2019)..
[2] A. Kwade et al., Nat. Energy 3 (2018) 290–300, https://doi.org/10.1038/s41560-018-0130-3.
[3] M. Li et al., Adv. Mater. 30 (2018) 1800561, https://doi.org/10.1002/adma.201800561.
[4] D. Deng, Energy Sci. Eng. 3 (2015) 385–418, https://doi.org/10.1002/ese3.95.
[5] J.B. Goodenough et al., J. Am. Chem. Soc. 135 (2013) 1167–1176, https://doi.org/10.1021/ja3091438.
[6] J. Liu et al., Nat. Energy 4 (2019) 180–186, https://doi.org/10.1038/s41560-019-0338-x.
[7] A. Manthiram et al., Adv. Energy Mater. 6 (2016) 1501010, https://doi.org/10.1002/aenm.201501010.
[8] N.S. Choi et al., Angew. Chem. Int. Ed. 51 (2012) 9994–10024, https://doi.org/10.1002/anie.201201429.
[9] Y. Ding et al., Electrochem. Energy Rev. 2 (2019) 1–28, https://doi.org/10.1007/s41918-018-0022-z.
[10] W. Li, B. Song, A. Manthiram, Chem. Soc. Rev. 46 (2017) 3006–3059, https://doi.org/10.1039/c6cs00875e.
[11] Z. Zhu et al., Nat. Energy 4 (2019) 1049–1058, https://doi.org/10.1038/s41560-019-0508-x.
[12] E. Zhao et al., Angew. Chem. Int. Ed. 58 (2019) 4323–4327, https://doi.org/10.1002/anie.201900444.
[13] S. Li et al., J. Am. Chem. Soc. 141 (2019) 12079–12086, https://doi.org/10.1021/jacs.9b05349.
[14] S.S. Zhang, Energy Storage Mater. 24 (2020) 247–254, https://doi.org/10.1016/j.ensm.2019.08.013.
[15] J.P. Pender et al., ACS Nano 14 (2020) 1243–1295, https://doi.org/10.1021/acsnano.9b04365.
[16] H. Maleki Kheimeh Sari et al., Adv. Energy Mater. 9 (2019) 1901597, https://doi.org/10.1002/aenm.201901597.
[17] L. Liang et al., Adv. Mater. Interfaces 7 (2020) 1901749, https://doi.org/10.1002/admi.201901749.
[18] T. Li et al., Electrochem. Energy Rev. 3 (2020) 43–80, https://doi.org/10.1007/s41918-019-00053-3.
[19] T. Hatsukade et al., ACS Appl. Mater. Interfaces 10 (2018) 38892–38899, https://doi.org/10.1021/acsami.8b13158.
[20] S.E. Renfrew et al., ACS Appl. Energy Mater. 2 (2019) 3762–3772, https://doi.org/10.1021/acsaem.9b00459.
[21] A.T.S. Freiberg et al., Electrochim. Acta 346 (2020) 136271, https://doi.org/10.1016/j.electacta.2020.136271.
[22] N. Yabuuchi et al., J. Am. Chem. Soc. 133 (2011) 4404–4419, https://doi.org/10.1021/ja108588y.
[23] S.-M. Bak et al., Chem. Mater. 25 (2013) 337–351, https://doi.org/10.1021/cm303096e.
[24] Y. Kim, J. Mater. Sci. 48 (2013) 8547–8551, https://doi.org/10.1007/s10853-013-7673-2.
[25] D.H. Seo et al., Nat. Chem. 8 (2016) 692–697, https://doi.org/10.1038/nchem.2524.
[26] G. Assat et al., Chem. Mater. 29 (2017) 9714–9724, https://doi.org/10.1021/acs.chemmater.7b03434.
[27] S. Sharifi-Asl et al., Adv. Energy Mater. 9 (2019) 1900551, https://doi.org/10.1002/aenm.201900551.
[28] S.-T. Myung et al., ACS Energy Lett. 2 (2017) 196–223, https://doi.org/10.1021/acsenergylett.6b00594.
[29] S.E. Renfrew et al., J. Am. Chem. Soc. 139 (2017) 17853–17860, https://doi.org/10.1021/jacs.7b08461.
[30] M. Si et al., Adv. Sci. 7 (2020) 1902538, https://doi.org/10.1002/advs.201902538.
[31] Y. Wei et al., J. Am. Chem. Soc. 137 (2015) 8364–8367, https://doi.org/10.1021/jacs.5b04040.
[32] H. Yu et al., Nano Lett. 16 (2016) 2907–2915, https://doi.org/10.1021/acs.nanolett.5b03933.
[33] B. Xiao et al., Nano Energy 34 (2017) 120–130, https://doi.org/10.1016/j.nanoen.2017.02.015.
[34] Y. Li et al., Nano Energy 71 (2020) 104643, https://doi.org/10.1016/j.nanoen.2020.104643.
[35] X. Ding et al., Nano Energy 61 (2019) 411–419, https://doi.org/10.1016/j.nanoen.2019.04.078.
[36] C. Chen et al., J. Power Sources 331 (2016) 91–99, https://doi.org/10.1016/j.jpowsour.2016.09.051.
[37] P. Yan et al., Nat. Energy 3 (2018) 600–605, https://doi.org/10.1038/s41560-018-0191-3.
[38] X. Ding et al., J. Mater. Chem. A 7 (2019) 11513–11519, https://doi.org/10.1039/c9ta02461a.
[39] Y. Huang et al., Electrochim. Acta 231 (2017) 294–299, https://doi.org/10.1016/j.electacta.2017.02.067.
[40] J. Huang et al., J. Electroanal. Chem. 823 (2018) 359–367, https://doi.org/10.1016/j.jelechem.2018.06.035.
[41] X.-D. Zhang et al., Adv. Mater. 30 (2018) 1801751, https://doi.org/10.1002/adma.201801751.
[42] L. Li et al., ACS Appl. Mater. Interfaces 8 (2016) 30879–30889, https://doi.org/10.1021/acsami.6b09197.
[43] T. He et al., ChemSusChem 11 (2018) 1639–1648.
[44] Q. Gan et al., ACS Appl. Mater. Interfaces 11 (2019) 12594–12604, https://doi.org/10.1021/acsami.9b04050.
[45] G.-L. Xu et al., Nat. Energy 4 (2019) 484–494, https://doi.org/10.1038/s41560-019-0387-1.

[46] S. Chen et al., ACS Appl. Mater. Interfaces 9 (2017) 29732–29743, https://doi.org/10.1021/acsami.7b08006.
[47] Y. Liu et al., Int. J. Energy Res. 44 (2020) 4717–4726, https://doi.org/10.1002/er.5253.
[48] S.S. Jan et al., Electrochim. Acta 149 (2014) 86–93, https://doi.org/10.1016/j.electacta.2014.10.093.
[49] J. Helbig, et al., J. Electrochem. Soc. 167 (2020)060519, https://doi.org/10.1149/1945-7111/ab8405..
[50] Y. Huang et al., ACS Appl. Mater. Interfaces 11 (2019) 16556–16566, https://doi.org/10.1021/acsami.9b01957.
[51] S. Chong et al., J. Power Sources 356 (2017) 153–162, https://doi.org/10.1016/j.jpowsour.2017.04.081.
[52] J. Li et al., Chem. Mater. 27 (2015) 7765–7773, https://doi.org/10.1021/acs.chemmater.5b03499.
[53] Y. Ma et al., Nano Energy 59 (2019) 184–196, https://doi.org/10.1016/j.nanoen.2019.02.040.
[54] M. Xu et al., J. Mater. Chem. A 3 (2015) 13933–13945, https://doi.org/10.1039/c5ta03676c.
[55] Z. Lin et al., Angew. Chem. Int. Ed. Engl. 59 (2020) 7778–7782, https://doi.org/10.1002/anie.202000628.
[56] D. Song et al., ACS Appl. Mater. Interfaces 7 (2015) 12864–12872, https://doi.org/10.1021/acsami.5b02373.
[57] Y.K. Sun et al., Nat. Mater. 8 (2009) 320–324, https://doi.org/10.1038/nmat2418.
[58] Y.K. Sun et al., Nat. Mater. 11 (2012) 942–947, https://doi.org/10.1038/nmat3435.
[59] S.E. Renfrew et al., ACS Appl. Mater. Interfaces 11 (2019) 34913–34921, https://doi.org/10.1021/acsami.9b09992.
[60] D. Pritzl et al., J. Electrochem. Soc. 166 (2019) A4056–A4066, https://doi.org/10.1149/2.1351915jes.
[61] S.H. Rosy et al., Chem. Mater. 31 (2019) 3840–3847, https://doi.org/10.1021/acs.chemmater.9b00875.
[62] J.D. Steiner et al., ACS Appl. Mater. Interfaces 11 (2019) 37885–37891, https://doi.org/10.1021/acsami.9b14729.
[63] P. Guan et al., J. Energy Chem. 43 (2020) 220–235, https://doi.org/10.1016/j.jechem.2019.08.022.
[64] Y. Liu et al., Small 15 (2019) 1901019, https://doi.org/10.1002/smll.201901019.
[65] B. Xiao, X. Sun, Adv. Energy Mater. 8 (2018) 1802057, https://doi.org/10.1002/aenm.201802057.
[66] S. Kalluri et al., Adv. Energy Mater. 7 (2017) 1601507, https://doi.org/10.1002/aenm.201601507.
[67] W. Liu et al., Angew. Chem. Int. Ed. 54 (2015) 4440–4457, https://doi.org/10.1002/anie.201409262.
[68] M. Wohlfahrt-Mehrens et al., J. Power Sources 127 (2004) 58–64, https://doi.org/10.1016/j.jpowsour.2003.09.034.
[69] C. Zhan et al., Energy Environ. Sci. 11 (2018) 243–257, https://pubs.rsc.org/en/content/articlepdf/2018/ee/c7ee03122j.
[70] S.-T. Myung et al., Chem. Mater. 17 (2005) 3695–3704, https://pubs.acs.org/doi/pdf/10.1021/cm050566s.
[71] C. Qin et al., Dalton Trans. 45 (2016) 9669–9675, https://doi.org/10.1039/C6DT01764A.
[72] G. Dai et al., RSC Adv. 6 (2016) 100841–100848, https://doi.org/10.1039/C6RA21903A.
[73] W. Cho et al., J. Power Sources 282 (2015) 45–50, https://doi.org/10.1016/j.jpowsour.2014.12.128.
[74] Y. Zhao et al., J. Alloys Compd. 715 (2017) 105–111, https://doi.org/10.1016/j.jallcom.2017.04.311.
[75] C.-H. Jo et al., Nano Res. 8 (2015) 1464–1479, https://doi.org/10.1007/s12274-014-0631-8.
[76] J.-M. Kim et al., Sci. Rep. 4 (2015) 4602, https://doi.org/10.1038/srep04602.
[77] B.-J. Chae, T. Yim, J. Power Sources 360 (2017) 480–487, https://doi.org/10.1016/j.jpowsour.2017.06.037.
[78] I.H. Son et al., Chem. Mater. 27 (2015) 7370–7379, https://doi.org/10.1021/acs.chemmater.5b03081.
[79] P.K. Nayak et al., Adv. Energy Mater. 8 (2018) 1702397, https://doi.org/10.1002/aenm.201702397.
[80] M.-J. Lee et al., Nano Lett. 14 (2014) 993–999, https://doi.org/10.1021/nl404430e.
[81] S. Pang et al., J. Power Sources 365 (2017) 68–75, https://doi.org/10.1016/j.jpowsour.2017.08.077.
[82] J.-M. Kim et al., Adv. Energy Mater. 10 (2020) 1903658, https://doi.org/10.1002/aenm.201903658.
[83] X. Liu et al., Electrochim. Acta 109 (2013) 52–58, https://doi.org/10.1016/j.electacta.2013.07.069.
[84] B. Song et al., J. Mater. Chem. A 1 (2013) 9954, https://doi.org/10.1039/c3ta11580a.
[85] P. Oh et al., Adv. Energy Mater. 4 (2014) 1400631, https://doi.org/10.1002/aenm.201400631.
[86] Y. Paik et al., Chem. Mater. 14 (2002) 5109–5115, https://doi.org/10.1021/cm0206385.
[87] S.-H. Kang et al., J. Electrochem. Soc. 153 (2006) A1186, https://doi.org/10.1149/1.2194764.
[88] C. Chen et al., J. Alloys Compds. 709 (2017) 708–716, https://doi.org/10.1016/j.jallcom.2017.03.225.
[89] P. Zhou et al., Nanoscale 8 (2016) 19263–19269, https://doi.org/10.1039/C6NR07438C.
[90] S.-H. Lee et al., J. Power Sources 234 (2013) 201–207, https://doi.org/10.1016/j.jpowsour.2013.01.045.
[91] Y.-K. Sun et al., Adv. Mater. 24 (2012) 1192–1196, https://doi.org/10.1002/adma.201104106.
[92] S.-W. Lee et al., J. Power Sources 360 (2017) 206–214, https://doi.org/10.1016/j.jpowsour.2017.05.042.
[93] A. Zhou et al., J. Power Sources 322 (2016) 10–16, https://doi.org/10.1016/j.jpowsour.2016.04.092.
[94] Z.-F. Tang et al., J. Alloys Compds. 693 (2017) 1157–1163, https://doi.org/10.1016/j.jallcom.2016.10.099.
[95] Y. Wu et al., ACS Energy Lett. 4 (2019) 656–665, https://doi.org/10.1021/acsenergylett.9b00032.
[96] S. Yang et al., ACS Appl. Mater. Interfaces 11 (2019) 36742–36750, https://doi.org/10.1021/acsami.9b12578.
[97] W. Cho et al., Electrochim. Acta 198 (2016) 77–83, https://doi.org/10.1016/j.electacta.2016.03.079.
[98] J.-H. Park et al., J. Mater. Chem. 22 (2012) 12574, https://doi.org/10.1039/c2jm16799a.
[99] J.-H. Park et al., J. Power Sources 244 (2013) 442–449, https://doi.org/10.1016/j.jpowsour.2012.11.111.
[100] J. Zhang et al., ACS Appl. Mater. Interfaces 6 (2014) 17965–17973, https://doi.org/10.1021/am504796n.
[101] M. Zhang et al., Electrochim. Acta 232 (2017) 80–88, https://doi.org/10.1016/j.electacta.2017.02.064.
[102] W.-J. Huang et al., J. Alloys Compd. 827 (2020) 154296, https://doi.org/10.1016/j.jallcom.2020.154296.
[103] J. Chen et al., Electrochim. Acta 312 (2019) 179–187, https://doi.org/10.1016/j.electacta.2019.04.153.
[104] Y. Tang et al., Chem. Soc. Rev. 44 (2015) 5926–5940, https://doi.org/10.1039/C4CS00442F.
[105] Y. Kim, Phys. Chem. Chem. Phys. 15 (2013) 6400, https://doi.org/10.1039/c3cp50567g.
[106] S.S. Zhang et al., ChemElectroChem 6 (2019) 1536–1541, https://doi.org/10.1002/celc.201801858.
[107] O. Tiurin et al., J. Power Sources 448 (2020) 227373, https://doi.org/10.1016/j.jpowsour.2019.227373.
[108] X. Zhang et al., J. Electron. Mater. 48 (2019) 4443–4451, https://doi.org/10.1007/s11664-019-07223-5.
[109] S. Ramakrishnan et al., J. Am. Chem. Soc. 142 (2020) 8522–8531, https://doi.org/10.1021/jacs.0c02859.
[110] E. Evenstein et al., Energy Storage Mater. 19 (2019) 261–269, https://doi.org/10.1016/j.ensm.2018.12.014.
[111] X. Wang et al., Adv. Energy Mater. 10 (2020) 1903864, https://doi.org/10.1002/aenm.201903864.
[112] K. Du et al., ACS Appl. Mater. Interfaces 8 (2016) 17713–17720, https://doi.org/10.1021/acsami.6b05629.
[113] Y. Su et al., ACS Appl. Mater. Interfaces 7 (2015) 25105–25112, https://doi.org/10.1021/acsami.5b05500.
[114] K. Araki et al., J. Power Sources 269 (2014) 236–243, https://doi.org/10.1016/j.jpowsour.2014.06.101.
[115] C. Hudaya et al., Solid State Ionics 256 (2014) 89–92, https://doi.org/10.1016/j.ssi.2014.01.016.
[116] M.M. Loghavi et al., J. Solid State Electrochem. 23 (2019) 2569–2578, https://doi.org/10.1007/s10008-019-04342-1.
[117] S. He et al., J. Alloys Compd. 799 (2019) 137–146, https://doi.org/10.1016/j.jallcom.2019.05.165.
[118] W. Hu et al., Electrochim. Acta 243 (2017) 105–111, https://doi.org/10.1016/j.electacta.2017.05.075.

[119] J. Wang et al., Phys. Chem. Chem. Phys. 17 (2015) 32033–32043, https://doi.org/10.1039/C5CP05319F.
[120] J. Zhang et al., Electrochim. Acta 209 (2016) 102–110, https://doi.org/10.1016/j.electacta.2016.05.066.
[121] F. Wang et al., Electrochim. Acta 295 (2019) 1017–1026, https://doi.org/10.1016/j.electacta.2018.09.050.
[122] A. Zhou et al., J. Power Sources 346 (2017) 24–30, https://doi.org/10.1016/j.jpowsour.2017.02.035.
[123] L. Shao et al., Electrochim. Acta 297 (2019) 742-748, https://doi.org/10.1016/j.electacta.2018.12.044..
[124] Z. Li et al., Energy Storage Mater. 29 (2020) 71–77, https://doi.org/10.1016/j.ensm.2020.03.031.
[125] S. Uchida et al., RSC Adv. 6 (2016) 67514–67519, https://doi.org/10.1039/C6RA10155K.
[126] J. Kim et al., Energy Environ. Sci. 11 (2018) 1449–1459, https://doi.org/10.1039/c8ee00155c.
[127] S. Zhao et al., Corros. Sci. 168 (2020) 108553, https://doi.org/10.1016/j.corsci.2020.108553.
[128] Y. Huang et al., ACS Appl. Mater. Interfaces 12 (2020) 19483–19494, https://doi.org/10.1021/acsami.0c01558.
[129] Y.K. Sun et al., Adv. Funct. Mater. 20 (2010) 485–491, https://doi.org/10.1002/adfm.200901730.
[130] P.K. Nayak et al., Adv. Energy Mater. 6 (2016) 1502398, https://doi.org/10.1002/aenm.201502398.
[131] U.H. Kim et al., Adv. Energy Mater. 9 (2019) 1803902, https://doi.org/10.1002/aenm.201803902.
[132] U.-H. Kim, et. al. Mater. Today 23 (2019) 26-36. https://doi.org/10.1016/j.mattod.2018.12.00..
[133] L. Qiu et al., Nano Energy 63 (2019) 103818, https://doi.org/10.1016/j.nanoen.2019.06.014.
[134] R.V. Chebiam et al., Electrochem. Commun. 3 (2001) 624–627, https://doi.org/10.1016/S1388-2481(01)00232-6.
[135] A. Manthiram et al., Nat. Commun. 11 (2020) 1–9, https://doi.org/10.1038/s41467-020-15355-0.
[136] Y. Xia et al., Nano Energy 49 (2018) 434–452, https://doi.org/10.1016/j.nanoen.2018.04.062.
[137] C. Wang et al., ACS Appl. Mater. Interfaces 11 (2019) 44036–44045, https://doi.org/10.1021/acsami.9b11452.
[138] A. Boulineau et al., Chem. Mater. 24 (2012) 3558–3566, https://doi.org/10.1021/cm301140g.
[139] M. Sathiya et al., Nat. Mater. 14 (2015) 230–238, https://doi.org/10.1038/nmat4137.
[140] Y. Gao et al., Electrochim. Acta 318 (2019) 513–524, https://doi.org/10.1016/j.electacta.2019.06.042.
[141] Y. Gao et al., RSC Adv. 6 (2016) 113275–113282, https://doi.org/10.1039/C6RA21637D.
[142] J.-Z. Kong et al., J. Alloys Compds. 694 (2017) 848–856, https://doi.org/10.1016/j.jallcom.2016.10.045.
[143] S. Sun et al., ChemSusChem 8 (2015) 2544–2550, https://doi.org/10.1002/cssc.201500143.
[144] C. Fu et al., J. Mater. Chem. A 7 (2019) 23149–23161, https://doi.org/10.1039/C9TA09327C.
[145] G.R. Li et al., Electrochim. Acta 78 (2012) 308–315, https://doi.org/10.1016/j.electacta.2012.05.142.
[146] X. Jiang et al., Electrochim. Acta 325 (2019) 134951, https://doi.org/10.1016/j.electacta.2019.134951.
[147] W. Li et al., Nat. Energy 5 (2020) 26–34, https://doi.org/10.1038/s41560-019-0513-0.
[148] J.W. Kim et al., J. Power Sources 254 (2014) 190–197, https://doi.org/10.1016/j.jpowsour.2013.12.119.
[149] Y.-Q. Lai et al., J. Power Sources 309 (2016) 20–26, https://doi.org/10.1016/j.jpowsour.2016.01.079.
[150] V.-C. Ho et al., J. Power Sources 450 (2020) 227625, https://doi.org/10.1016/j.jpowsour.2019.227625.
[151] S. Hashigami et al., ChemistrySelect 4 (2019) 8676–8681, https://doi.org/10.1002/slct.201900874.
[152] S. Xia et al., J. Energy Chem. 45 (2020) 110–118, https://doi.org/10.1016/j.jechem.2019.09.023.
[153] B. Song et al., ACS Appl. Mater. Interfaces 9 (2017) 9718–9725, https://doi.org/10.1021/acsami.7b00070.
[154] C.-W. Wang et al., ACS Appl. Energy Mater. 3 (2020) 2593–2603, https://doi.org/10.1021/acsaem.9b02291.
[155] H. Kim et al., Adv. Mater. 28 (2016) 4705–4712, https://doi.org/10.1002/adma.201506256.
[156] X. Cheng et al., Nano Energy 62 (2019) 30–37, https://doi.org/10.1016/j.nanoen.2019.05.021.
[157] Y. Liu et al., ACS Nano 13 (2019) 11891–11900, https://doi.org/10.1021/acsnano.9b05960.
[158] Q. Li et al., Adv. Funct. Mater. 29 (2019) 1806706, https://doi.org/10.1002/adfm.201806706.
[159] H.-J. Noh et al., J. Power Sources 233 (2013) 121–130, https://doi.org/10.1016/j.jpowsour.2013.01.063.
[160] Z. Feng et al., Chem. Eng. J. 382 (2020) 122959, https://doi.org/10.1016/j.cej.2019.122959.
[161] R. Zhao et al., J. Alloys Compds. 724 (2017) 1109–1116, https://doi.org/10.1016/j.jallcom.2017.05.331.
[162] W.-G. Ryu et al., Ceram. Int. 45 (2019) 13942–13950, https://doi.org/10.1016/j.ceramint.2019.04.092.
[163] Q. Xie et al., Chem. Mater. 32 (2020) 7413–7424, https://doi.org/10.1021/acs.chemmater.0c02374.
[164] S.W. Doo et al., ACS Appl. Energy Mater. 2 (2019) 6246–6253, https://doi.org/10.1021/acsaem.9b00786.
[165] W. Gu et al., ACS Appl. Mater. Interfaces 12 (2020) 1937–1943, https://doi.org/10.1021/acsami.9b20030.
[166] Y. Xiao et al., Joule 3 (2019) 1252–1275, https://doi.org/10.1016/j.joule.2019.02.006.
[167] H. Qi et al., Int. J. Electrochem. Sci 12 (2017) 5836–5844, https://doi.org/10.20964/2017.07.01.
[168] P. Liu et al., Ceram. Int. 45 (2019) 18398–18405, https://doi.org/10.1016/j.ceramint.2019.06.055.
[169] A. Zhou et al., J. Power Sources 362 (2017) 131–139, https://doi.org/10.1016/j.jpowsour.2017.06.050.
[170] N. Wu et al., J. Alloys Compds. 665 (2016) 48–56, https://doi.org/10.1016/j.jallcom.2016.01.044.
[171] L. Wang et al., Electrochim. Acta 222 (2016) 806–813, https://doi.org/10.1016/j.electacta.2016.11.041.
[172] L. Zhou et al., J. Alloys Compds. 724 (2017) 991–999, https://doi.org/10.1016/j.jallcom.2017.05.328.
[173] E. Zhao et al., Chem. Commun. 51 (2015) 9093–9096, https://doi.org/10.1039/c5cc00383k.
[174] X. Huang et al., J. Solid State Electrochem. 19 (2015) 805–812, https://doi.org/10.1007/s10008-014-2661-2.
[175] C.-C. Yang et al., Appl. Surf. Sci. 399 (2017) 670–681, https://doi.org/10.1016/j.apsusc.2016.12.121.
[176] H. Liu et al., J. Mater. Chem. A 3 (2015) 2634–2641, https://doi.org/10.1039/c4ta04823g.
[177] J. Zhu et al., J. Alloys Compds. 773 (2019) 112–120, https://doi.org/10.1016/j.jallcom.2018.09.237.
[178] Z. Chen et al., Adv. Energy Mater. 8 (2018) 1801573, https://doi.org/10.1002/aenm.201801573.
[179] Z. Chen et al., J. Power Sources 402 (2018) 263–271, https://doi.org/10.1016/j.jpowsour.2018.09.049.
[180] H. Tong et al., J. Alloys Compds. 764 (2018) 44–50, https://doi.org/10.1016/j.jallcom.2018.06.020.
[181] L. Liang et al., J. Power Sources 328 (2016) 422–432, https://doi.org/10.1016/j.jpowsour.2016.08.014.
[182] J. Zhang et al., ACS Appl. Mater. Interfaces 11 (2019) 15507–15516, https://doi.org/10.1021/acsami.9b00389.
[183] Y. Liu et al., J. Power Sources 403 (2018) 27–37, https://doi.org/10.1016/j.jpowsour.2018.09.082.
[184] B. Shen et al., Electrochem. Commun. 83 (2017) 106–109, https://doi.org/10.1016/j.elecom.2017.09.002.
[185] Z. Wang et al., Appl. Surf. Sci. 370 (2016) 437–444, https://doi.org/10.1016/j.apsusc.2016.02.139.
[186] Y. Liu et al., Electrochim. Acta 147 (2014) 696–703, https://doi.org/10.1016/j.electacta.2014.10.011.
[187] Y. Chen et al., ACS Appl. Mater. Interfaces 6 (2014) 16888–16894, https://doi.org/10.1021/am504412n.
[188] J.-H. Shim et al., Chem. Mater. 27 (2015) 3273–3279, https://doi.org/10.1021/acs.chemmater.5b00159.
[189] A. Zhou et al., ACS Appl. Mater. Interfaces 8 (2016) 34123–34131, https://doi.org/10.1021/acsami.6b11630.
[190] Y.-D. Xu et al., Electrochim. Acta 268 (2018) 358–365, https://doi.org/10.1016/j.electacta.2018.02.049.

[191] H. Zou et al., ACS Appl. Mater. Interfaces 8 (2016) 21407–21416, https://doi.org/10.1021/acsami.6b07742.
[192] M. Kamata et al., J. Electrochem. Soc. 143 (1996) 1866–1870, https://doi.org/10.1149/1.1836916.
[193] Y. Han et al., ACS Energy Lett. 5 (2020) 2421–2433, https://doi.org/10.1021/acsenergylett.0c01032.
[194] Q. Xue et al., J. Mater. Chem. A 2 (2014) 18613–18623, https://doi.org/10.1039/C4TA04024D.
[195] Y. Cao et al., ACS Appl. Mater. Interfaces 10 (2018) 18270–18280, https://doi.org/10.1021/acsami.8b02396.
[196] J.H. Shim et al., ACS Appl. Mater. Interfaces 9 (2017) 18720–18729, https://doi.org/10.1021/acsami.7b02654.
[197] Y. Li et al., J. Energy Chem. 27 (2018) 559–564, https://doi.org/10.1016/j.jechem.2017.11.004.
[198] H. Yang et al., ACS Appl. Mater. Interfaces 11 (2019) 8556–8566, https://doi.org/10.1021/acsami.8b21621.
[199] W. Luo et al., J. Alloys Compds. 810 (2019) 151786, https://doi.org/10.1016/j.jallcom.2019.151786.
[200] C. Yang et al., ACS Appl. Mater. Interfaces 9 (2017) 12408–12415, https://doi.org/10.1021/acsami.6b16741.
[201] D. Ren et al., J. Power Sources 447 (2020) 227344, https://doi.org/10.1016/j.jpowsour.2019.227344.
[202] K. Nie et al., J. Power Sources 470 (2020), https://doi.org/10.1016/j.jpowsour.2020.228423 228423.
[203] F. Wu et al., ACS Appl. Mater. Interfaces 8 (2016) 23095–23104, https://doi.org/10.1021/acsami.6b07431.
[204] T.H. Le et al., Polymer 9 (2017) 150, https://doi.org/10.3390/polym9040150..
[205] S. Zhao et al., ACS Appl. Mater. Interfaces 10 (2018) 33260–33268, https://doi.org/10.1021/acsami.8b11471.
[206] S. Hu et al., Adv. Energy Mater. 9 (2019) 1901795, https://doi.org/10.1002/aenm.201901795.
[207] D. Wang et al., ACS Appl. Mater. Interfaces 10 (2018) 41802–41813, https://doi.org/10.1021/acsami.8b16319.
[208] X. Zhang et al., Electrochim. Acta 193 (2016) 96–103, https://doi.org/10.1016/j.electacta.2016.02.065.
[209] B.-B. Lim et al., ACS Energy Lett. 1 (2016) 283–289, https://doi.org/10.1021/acsenergylett.6b00150.
[210] J.-Y. Liao et al., J. Power Sources 282 (2015) 429–436, https://doi.org/10.1016/j.jpowsour.2015.02.078.
[211] D. Mohanty et al., Sci. Rep. 6 (2016) 26532, https://doi.org/10.1038/srep26532.
[212] B. Wu et al., Adv. Funct. Mater. 28 (2018) 1803392, https://doi.org/10.1002/adfm.v28.37.
[213] J.-R. He et al., RSC Adv. 4 (2014) 2568–2572, https://doi.org/10.1039/c3ra45115a.
[214] X. Wang et al., Energy Environ. Sci. 8 (2015) 1889–1904, https://doi.org/10.1039/c5ee01254f.
[215] Y.S. Jung et al., J. Electrochem. Soc. 158 (2011) A1298, https://doi.org/10.1149/2.030112jes.
[216] A.M. Wise et al., Chem. Mater. 27 (2015) 6146–6154, https://doi.org/10.1021/acs.chemmater.5b02952.
[217] A.M. Wise et al., J. Power Sources 247 (2014) 57–69, https://doi.org/10.1016/j.jpowsour.2013.08.042.
[218] J. Xie et al., ACS Nano 11 (2017) 7019–7027, https://doi.org/10.1021/acsnano.7b02561.
[219] X. Li et al., Energy Environ. Sci. 7 (2014) 768–778, https://doi.org/10.1039/c3ee42704h.
[220] J.-Z. Kong et al., J. Alloys Compds. 799 (2019) 89–98, https://doi.org/10.1016/j.jallcom.2019.05.330.
[221] S. Lee et al., Appl. Surf. Sci. 458 (2018) 864–871, https://doi.org/10.1016/j.apsusc.2018.07.158.
[222] J.W. DuMont et al., J. Phys. Chem. C 119 (2015) 14603–14612, https://doi.org/10.1021/jp512074n.
[223] Y.-K. Sun et al., J. Phys. Chem. B 110 (2006) 6810–6815, https://doi.org/10.1021/jp0571473.
[224] Y.-K. Sun et al., J. Am. Chem. Soc. 127 (2005) 13411–13418, https://doi.org/10.1021/ja053675g.
[225] B. Michalak et al., J. Phys. Chem. C 121 (2017) 211–216, https://doi.org/10.1021/acs.jpcc.6b11184.
[226] H. Lee et al., ACS Energy Lett. 3 (2018) 2921–2930, https://doi.org/10.1021/acsenergylett.8b01819.
[227] J. Betz et al., Adv. Energy Mater. 9 (2019) 1900574, https://doi.org/10.1002/aenm.201900574.
[228] J.-L. Shi et al., Adv. Mater. 30 (2018) 1705575, https://doi.org/10.1002/adma.201705575.
[229] M. Li et al., Chem. Soc. Rev. 49 (2020) 1688–1705, https://doi.org/10.1039/c8cs00426a.
[230] C. Cui et al., J. Am. Chem. Soc. 142 (2020) 8918–8927, https://doi.org/10.1021/jacs.0c02302.
[231] J. Kim et al., Adv. Energy Mater. 8 (2018) 1702028, https://doi.org/10.1002/aenm.201702028.